8-2012

Development And Implementation Of A Remote Audit Tool For High Dose Rate (Hdr) 192Ir Brachytherapy Using Optically Stimulated Luminescence Dosimetry

Kevin Casey

DEVELOPMENT AND IMPLEMENTATION OF A REMOTE AUDIT TOOL FOR HIGH DOSE RATE (HDR) ^{192}IR BRACHYTHERAPY USING OPTICALLY STIMULATED LUMINESCENCE DOSIMETRY

By

Kevin Casey, B.S.

APPROVED:

_____

David Followill, Ph.D.
Supervisory Professor

_____

Paola Alvarez, M.S.

_____

Kenneth Hess, Ph.D.

_____

Rebecca Howell, Ph.D.

_____

Stephen Kry, Ph.D.

_____

Ann Lawyer, M.S.

APPROVED:

_____

Michelle C. Barton, Ph.D.
Dean, The University of Texas
Health Science Center at Houston
Graduate School of Biomedical Sciences

_____

Michael R. Blackburn, Ph.D.
Dean, The University of Texas
Health Science Center at Houston
Graduate School of Biomedical Sciences

DEVELOPMENT AND IMPLEMENTATION OF A REMOTE AUDIT TOOL FOR HIGH DOSE RATE (HDR) ^{192}IR BRACHYTHERAPY USING OPTICALLY STIMULATED LUMINESCENCE DOSIMETRY

A
THESIS

Presented to the Faculty of

The University of Texas
Health Science Center at Houston
Graduate School of Biomedical Sciences
and
The University of Texas
M.D. Anderson Cancer Center

In Partial Fulfillment

of the Requirements

for the Degree of

MASTER OF SCIENCE

By

Kevin Casey, B.S.

Houston, TX
August, 2012

Acknowledgements

I must first thank my advisor, Dr. David Followill, for the opportunity to work on a project that I hope and believe will have a lasting impact on the RPC's ability to carry out its crucially important mission. His patient guidance throughout this entire process has been invaluable and his leadership of the RPC promotes a tremendous culture of teamwork, cooperation, and discovery.

I would also like to thank the members of my thesis committee: Dr. Kenneth Hess, Dr. Rebecca Howell, Dr. Stephen Kry, Ms. Ann Lawyer, and especially Ms. Paola Alvarez. Paola spent countless hours teaching me about OSLDs, helping me to analyze data, and encouraging me in general. Each committee member made valuable suggestions that helped the project along or helped point me in new and interesting directions. Dr. Firas Mourtada also offered many helpful suggestions, both as an early committee member and even continuing to do so after moving to a new institution.

The entire staff of the RPC has been extremely helpful. Sarah Willis was absolutely vital to the success of this project, continually helping me to get OSLD measurements and doing so with amazing efficiency and uncommon cheerfulness. Paige Summers offered great advice on the thesis writing process. Many others at the RPC contributed suggestions, material support, or both.

Laura Rechner at M.D. Anderson and Dr. Scott Davidson at The Methodist Hospital were absolutely crucial in my quest to learn about and realize a project involving HDR brachytherapy. Without their help, this project could have never even gotten off the ground. The same goes for John Costales, who machined the phantom prototypes with precision and speed with only my simplistic drawings as guidance.

I'd also like to thank my fellow students at the RPC, especially Jennelle Bergene, Mitchell Carroll, and Kevin Vredevoogd for many helpful discussions covering everything from specific minute details of my project to the process of science in general.

Finally, the biggest thanks go to my amazing wife Sara for being unbelievably patient, supportive, and encouraging throughout my entire graduate school experience.

DEVELOPMENT AND IMPLEMENTATION OF A REMOTE AUDIT TOOL FOR HIGH DOSE RATE (HDR) ^{192}IR BRACHYTHERAPY USING OPTICALLY STIMULATED LUMINESCENCE DOSIMETRY

Publication Number: _____

Kevin Casey, B.S.

Supervisory Professor: David Followill, Ph.D.

This work aimed to create a mailable and OSLD-based phantom with accuracy suitable for RPC audits of HDR brachytherapy sources at institutions participating in NCI-funded cooperative clinical trials. An 8 × 8 × 10 cm^3 prototype with two slots capable of holding nanoDot Al_2O_3:C OSL dosimeters (Landauer, Glenwood, IL) was designed and built. The phantom has a single channel capable of accepting all ^{192}Ir HDR brachytherapy sources in current clinical use in the United States. Irradiations were performed with an ^{192}Ir HDR source to determine correction factors for linearity with dose, dose rate, and the combined effect of irradiation energy and phantom construction. The uncertainties introduced by source positioning in the phantom and timer resolution limitations were also investigated. It was found that the linearity correction factor was $K_L = (-9.43 \times 10^{-5} \times dose) + 1.009$ where *dose* is in cGy, which differed from that determined by the RPC for the same batch of dosimeters under ^{60}Co irradiation. There was no significant dose rate effect. Separate energy+block correction factors were determined for both models of ^{192}Ir sources currently in clinical use and these vendor-specific correction factors differed by almost 2.6%. For Nucletron sources, this correction factor was 1.026±0.004 (99% Confidence Interval) and for Varian sources it was 1.000±0.007 (99% CI). Reasonable deviations in source positioning within the phantom and the limited resolution of the source timer had insignificant effects on the ability to measure dose. Overall measurement uncertainty of the system was estimated to be ±2.5% for both Nucletron and Varian source audits (95% CI). This uncertainty was sufficient to establish a ±5% acceptance criterion for source strength audits under a formal RPC audit program. Trial audits of eight participating institutions resulted in an average RPC-to-institution dose ratio of 1.000 with a standard deviation of 0.011.

Table of Contents

List of Figures

List of Tables

List of Equations

1. Introduction

1.1. Statement of the Problem

1.1.1. General Problem Area

If the therapeutic goals of radiation therapy are to be met, the need for accurate dosimetry in the application of high dose-rate (HDR) brachytherapy is paramount. A typical 10 Ci ^{192}Ir source may have a dose rate in excess of seven Gray per minute at a point 1 cm away from the source, leaving little room for error in the achievement of desired dose distributions. Just as in external beam radiation therapy (EBRT), satisfactory clinical outcomes in brachytherapy procedures require strict adherence to planned dose distributions. Substantial deviations from planned doses may result in reduced local control of the tumor or unacceptable damage to normal critical organs.

Furthermore, HDR brachytherapy has been employed in a number of recent National Cancer Institute (NCI) funded multi-institutional cooperative clinical trials[1-3]. The cooperative groups' requirements that participating institutions be rigorously credentialed prior to participation underscore the need for effective and efficient brachytherapy QA procedures. The success of such multicenter trials relies on the consistency and comparability of patient treatment across all participating institutions. Thus, the ability to calculate and deliver a prescribed dose must be evaluated and monitored carefully for trials that may span dozens or even hundreds of individual clinics.

1.1.2. Specific Problem Area

The Radiological Physics Center (RPC) is an organization funded by the NCI and set up specifically to monitor dosimetry practices at institutions participating in cooperative clinical trials. The RPC employs a variety of quality assurance audit tools to accomplish this goal. One of the primary audit activities of the RPC is a mailed optically-stimulated luminescence dosimetry (OSLD) program[4] for independent verification of an institution's external beam radiation therapy (EBRT) reference calibration. However, the RPC currently lacks a similar tool for any kind of remote brachytherapy audits, including HDR brachytherapy. As a result, the RPC's HDR credentialing procedures currently consist of questionnaires, independent plan reviews, and occasional site visits to participating institutions which are both time-consuming and expensive.

Optically-stimulated luminescence dosimeters (OSLDs) have certain features that make them a promising candidate to form the basis of a remote audit program for HDR brachytherapy. Homnick *et al.*[5] have demonstrated that post-irradiation exposure to reasonable temperature and humidity changes does not significantly affect dosimeter readings. Aguirre *et al.*[6] compared OSLD to thermoluminescent dosimeter (TLD) results and developed a method for working with the large numbers of individual OSLD nanoDots required for the RPC's EBRT audit program. Several recent RPC studies have demonstrated the high accuracy and acceptably low uncertainty of the OSLD system versus both the older TLD standard and ion chamber measurements[5-8]. Additionally, an OSLD packaging under the brand name nanoDot and supplied by Landauer, Inc. (Glenwood, IL) contains a thin (approximately 0.3 mm thick and 5 mm in diameter) sheet of Al_2O_3:C material which may be approximated as planar; this geometry makes this particular dosimeter suitable for measurements of brachytherapy sources which have high spatial dose gradients.

Although both single-crystal[9] and planar-type[10, 11] OSL dosimeters have been characterized for ^{192}Ir irradiation, there is a lack of published data in the literature regarding the use of OSLDs as remote audit dosimeters for HDR brachytherapy. Ochoa *et al.*[12] and Roué *et al*.[13] designed similar systems for performing source strength and dose calculation audits, however in both works the phantom designs relied on TLD powder-filled capsules. Since steep spatial dose gradients are a defining characteristic of ^{192}Ir HDR sources, TLD capsules with a thickness of perhaps 2-3 mm are not ideal for measuring dose in the region around such sources[14]. On the other hand, an OSLD-based mailable tool using near-planar nanoDot dosimeters sidesteps this limitation. A novel phantom with the ability to provide accurate HDR source strength audits would be an important addition to the RPC's ability to adequately credential institutions performing HDR under the auspices of NCI-funded clinical trials.

1.2. Background

1.2.1. High Dose-Rate Brachytherapy

Brachytherapy – from the Greek *brachys* meaning "short-distance" and thus meaning "treatment at a short distance" – is a type of radiation therapy involving the use of sealed radioactive sources placed inside the body in close proximity to the target. These sources may be applied by intracavitary, interstitial, or intravascular means. The first brachytherapy treatments for cancer began shortly after Marie and Pierre Curie isolated radium in 1898[15]. The use of both radium

needles and radon-filled glass capillary tubes proceeded throughout the first half of the 20th century until concerns about personnel doses and the rise of megavoltage external beam therapy caused the popularity of brachytherapy in general to wane in the 1950s and 60s[16].

However, the new availability of man-made radioisotopes following the advent of civilian nuclear energy and the invention of remote afterloading technology began to revitalize brachytherapy in the 1960s. Originally introduced by Walstam in 1962 and Henschke *et al.* in 1964[16], and utilized and refined early on at Memorial Sloan-Kettering Cancer Center[15], remote afterloading addressed many of the shielding and personnel exposure concerns inherent to brachytherapy at the time while also making high dose-rate (HDR) brachytherapy possible.

The dominant radioisotope in use today in HDR procedures, defined by ICRU Report 38[17] as any brachytherapy procedure with a dose rate of 2.0 cGy/min or higher, is Iridium-192. ^{192}Ir has a half-life of 73.83 days and decays via β decay (~95% branching ratio) to excited states of ^{192}Pt and electron capture (~5%) to excited states of ^{192}Os[18]. It has a complex emission spectrum but the average energy of emitted photons is commonly assumed to be around 370 keV[19]. A major advantage is its high specific activity such that seeds with dimensions on the order of millimeters can be manufactured and achieve acceptably high dose rates.

High dose-rate brachytherapy has several advantages when compared to low dose-rate (LDR) brachytherapy. HDR treatments are typically performed on an outpatient basis and require far less time than LDR treatments, improving patient throughput and reducing cost[20]. Unlike a patient with permanent LDR seed implants, a patient treated with HDR does not continue to emit radiation after leaving the treatment center. Modern planning and afterloading techniques also enable more precise dose distribution than LDR implants[21] and afterloaders reduce the radiation exposure to hospital personnel to negligible levels. On the other hand, LDR techniques may have certain radiobiological advantages which are lost with higher dose rates, and the relative efficacy of each remains unresolved.

Similarly, HDR brachytherapy offers advantages that are unmatched by external beam radiation therapy (EBRT). By definition, brachytherapy sources are placed as close to the tumor as possible. With precise physical placement and the rapid fall-off of dose due to the inverse square law, brachytherapy offers increased concentration of dose in the tumor and better sparing of surrounding organs at risk than do even the most conformal EBRT techniques. Furthermore, a

typical HDR treatment regimen which requires perhaps one week, compared to a fractionated EBRT schedule spread over four to six weeks, prohibits significant tumor-cell proliferation during treatment itself[20]. On the other hand, HDR brachytherapy is in practice accessible to relatively few tumor sites compared to EBRT and can treat primary tumors only without any chance of including involved regional lymph nodes.

Clinical usage of high dose-rate brachytherapy for certain cancers has been increasing in recent years. In 1999, 13.3% of patients with carcinoma of the cervix in the United States received HDR brachytherapy[22]. By 2010, that number had increased to 85%[23] as HDR largely supplanted LDR in the treatment of cervical cancer. Similarly, a survey of breast cancer patients treated between 2002 and 2007 showed a tenfold increase in the number receiving brachytherapy (generally high dose-rate accelerated partial breast irradiation) over that time period[24]. Overall, Nag *et al.*[25] found just 15.6% of radiotherapy facilities providing afterloaded HDR brachytherapy in 1995. A 2008 survey[26] of radiation oncology residents, on the other hand, found that 95.9% reported receiving training in HDR brachytherapy.

1.2.2. Radiological Physics Center

The RPC was founded in 1968[27] under the advice of the American Association of Physicists in Medicine (AAPM), which still acts as an advisory body for the center. Since that time, the National Cancer Institute (NCI) has continually provided funding to the RPC to support its mission of ensuring dosimetric accuracy and consistency among institutions participating in NCI-funded cooperative clinical trials. In accordance with this mission, the RPC works closely with the Cooperative Groups and other quality assurance centers through the Advanced Technologies Consortium.

A major component of the RPC's quality assurance outreach program is the mailed dosimeter program, initiated in 1977 using thermoluminescent dosimeters (TLDs) in a specially-designed miniphantom[28]. The program was transitioned to an OSLD standard in 2010[5]. Examples of the acrylic miniphantoms used for the external beam program are shown in Figure 1.1. The new OSLD system was shown by Aguirre *et al.*[7] to have an uncertainty of 1.8% (1 standard deviation) under standard external-beam irradiation conditions, exceeding the accuracy of the older TLD system. Disagreement between the institution's reported dose and the RPC's dosimeter readings of 5% or more triggers an on-site audit by RPC staff in order to investigate the discrepancy. In 2010,

the RPC's external beam audit program monitored more than 1,700 institutions in the United States and internationally, comprising approximately 14,000 individual beam audits per year[29]. The program has been highly successful at uncovering discrepancies, with approximately 15-20% of institutions having one or more unacceptable measurements in any given year[30].

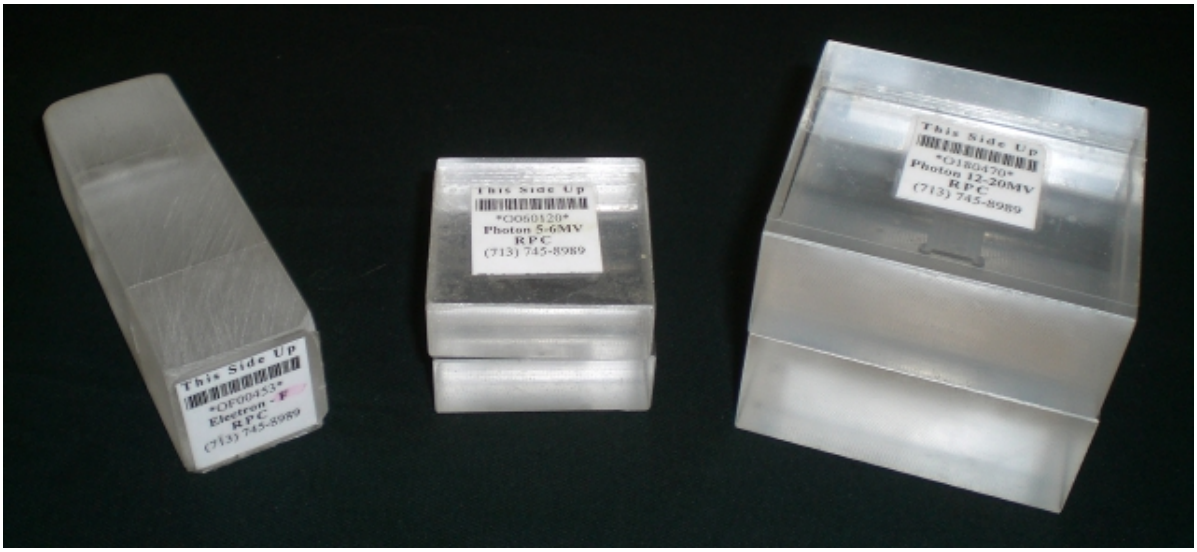

Figure 1.1: Examples of the acrylic blocks used for the RPC's external beam remote audit program. From left to right: an electron block, a photon block for 5-6 MV, and a photon block for 12-20 MV.

In contrast, and despite HDR's growing use in clinical trials, the RPC does not currently have a mailable audit system for HDR brachytherapy. The current extent of HDR audit activities at the RPC is measurements of source strength during on-site visits (approximately 20 per year), physicist questionnaires, plan reviews, and institutional completion of a standard benchmark plan[27]. On-site source strength measurements provide an accurate independent evaluation of an institution's radioactive source, but are infrequent, expensive, time-consuming, and omit important steps in the patient treatment workflow. The RPC's brachytherapy treatment planning benchmarks have uncovered institutional misunderstandings and incorrect brachytherapy dosimetry parameters[31], but a mailable tool that provides an accurate audit of source strength as well as a tangible evaluation of both planning and treatment delivery – analogous to the current external beam audit program – is desirable.

1.2.3. Optically Stimulated Luminescence

1.2.3.1. Developmental History

The potential for using optically-stimulated luminescence as a dosimetry tool was first recognized in the 1950s[32]. However, the difficulties in identifying materials with suitable properties slowed research in OSLDs for much of the 20th century. Various compounds were proposed and some even used for specialty purposes, however drawbacks such as strong fading, unacceptable band-gap widths, high effective atomic numbers, low sensitivity, manufacturing difficulties, or some combination thereof rendered each new compound largely unsuitable for medical dosimetry use[33]. It was not until Al_2O_3:C was identified and developed in the early 1990s[34] that a practical and accurate OSLD material became available. Al_2O_3 was initially proposed as a thermoluminescent (TL) material[35] in 1957 and various dopants were investigated through the years[33]. The advent of carbon-doped aluminum oxide in the late 1980s[34], initially intended as an ultra-sensitive thermoluminescent material, elevated the sensitivity of the compound to levels suitable for accurate medical dosimetry. High sensitivity and other desirable properties have resulted in Al_2O_3:C becoming the dominant OSL material for dosimetric measurements in use today. The first commercially-available OSLD was introduced by Landauer in 1998. Today OSLDs are available in a variety of physical formats intended for different applications. One such packaging, the nanoDot by Landauer, is a small OSLD in a light-tight case intended for medical dosimetry; nanoDots were used extensively in this work and are discussed at length below.

1.2.3.2. OSL Mechanism

The thermoluminescent and optically-stimulated luminescence phenomena are understood in the context of an energy band model of electrons in crystalline solids. Specifically, the energy bands that are important to TL and OSL processes are known as the valence and conduction bands. Electrons in the valence band are essentially bound to the lattice structure, whereas electrons in the conduction band are free to move within the lattice[36]. Between these two levels sits the "forbidden band" or band gap, in which no electrons can exist[37]. Ionizing radiation passing through the crystal with sufficient energy can excite electrons from the valence band into the conduction band, leaving behind a positively-charged hole in the valence band. This is depicted as Process 1 in Figure 1.2. Electrons in the conduction band can subsequently fall back to the valence band and recombine with holes, or they can fall into localized energy levels present within the band gap[38].

These localized energy levels, or “traps”, exist in the energy band structure due to the introduction of impurities in the crystal lattice. It is the trapping of electrons in these localized levels, and their subsequent liberation, that gives rise to both the TL and OSL phenomena. In an ideal TL or OSL material, the number of electrons trapped in intermediate energy levels between the valence and conduction bands is directly proportional to the radiation dose absorbed by the material.

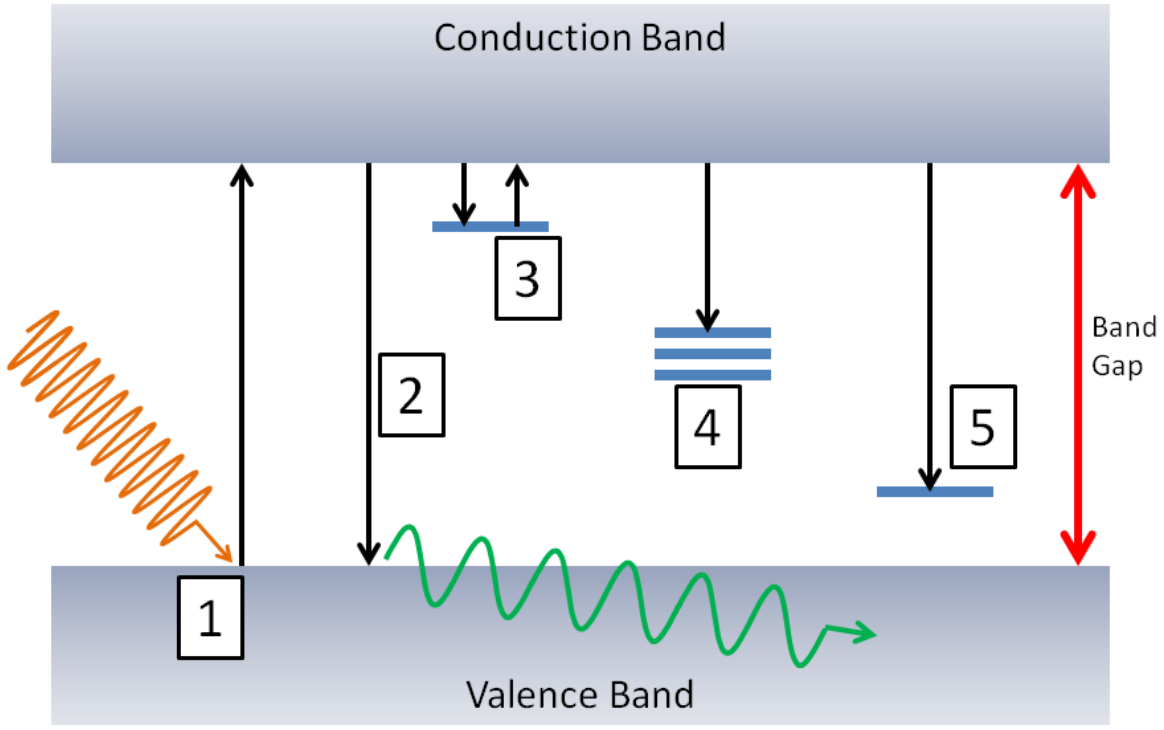

Figure 1.2: Energy band diagram of a dosimetric OSL material.

An electron elevated to the conduction band is free to move within the lattice structure but will soon fall into a trap or recombine with a hole. The process by which electrons fall from the conduction band and recombine with a hole without being caught in a trap is called prompt recombination and produces radioluminescence (RL). Prompt recombination and subsequent RL is depicted as Process 2 in Figure 1.2. There have been attempts to use the RL signal produced by Al_2O_3:C as a real-time active dosimeter[39, 40], but this approach faces difficulties since prompt recombination competes with all other trapping processes[38]. Mathematical models of the RL signal during dosimeter irradiation have been developed[41].

Electrons in the conduction band may also fall into so-called “shallow” traps – localized energy levels close to the conduction band[38]. This is indicated as Process 3 in Figure 1.2. The proximity of shallow traps to the conduction band makes it relatively easy for electrons to escape

these levels and jump back to the conduction band. In fact, the gap between shallow traps and the conduction band is so narrow that the probability of an electron escaping from the traps is considerable even at room temperatures. This results in a gradual loss of stored signal in the dosimeter, as electrons excited to the shallow traps by irradiation migrate to the conduction band and recombine after irradiation ends. For this reason, it is customary to wait for a period of hours or even days after irradiation before reading the signal stored in an OSLD. Another implication of shallow trap emptying at room temperature is that actual OSL signal can briefly rise upon first being read. This is due to electrons liberated from "dosimetric" traps during the reading process falling into empty shallow traps. As the shallow traps saturate with charges, OSL signal gradually rises and eventually stabilizes.

Another competing process is the capture of conduction-band electrons by "deep" traps[38], labeled as Process 5 in Figure 1.2. In contrast to shallow traps, the energy gap between the deep traps and the conduction band is sufficiently large enough to make it unlikely that normal readout procedures will liberate electrons in these traps. This has the unwanted effect of making the dosimeter's sensitivity dependent in some way on its irradiation history. In its initial unirradiated state, the deep traps in a sample of material are vacant. As the dosimeter is irradiated, charges fall into the deep traps and are unlikely to ever be liberated, resulting in the removal of the deep traps as a competing process to normal dosimetric functioning. This has the effect of making the dosimeter slightly more sensitive over time.

The most important traps in an OSL material are those located between shallow and deep traps in the energy spectrum. These are known as the "dosimetric" traps, and they are the energy levels exploited for the purposes of dosimetry. This process is labeled as Process 4 in Figure 1.2. The intermediate energy of dosimetric traps means that they are acceptably stable at room temperature yet do not require extremely high temperatures (in the case of TL) or high-frequency light (in the case of OSL) in order to be liberated.

1.2.3.3. Al_2O_3:C

Aluminum oxide doped with carbon is easily the most important OSL dosimeter material in use today. Al_2O_3 crystals can be grown using a number of different methods[33] and when grown in the presence of carbon, all of these methods produce Al_2O_3:C with numerous oxygen vacancies in the lattice structure. When an oxygen vacancy is occupied by two electrons it is known as an F-

center, and when it is occupied by a single electron it is known as an F^+-center, being positively-charged with respect to the overall lattice[33]. Concentrations of the two types of defects in typical commercially-available dosimeters are approximately 10^{17} cm^{-3} and 10^{15}-10^{16} cm^{-3}, respectively[34]. The F- and F^+-centers act as recombination centers and are responsible for the emission of light by OSL. Electrons liberated from trapping centers by incident light recombine with the positively-charged F^+-centers. The result is an excited state of an F-center, which relaxes to its ground state. It is this relaxation that produces the emitted observed luminescence centered at 420 nm[38, 42].

Al_2O_3:C has many properties which make it an excellent choice for medical dosimetry. Its response has been shown to be linear up to 50 Gy[43]. Because of its very high sensitivity, only a small proportion of the total trapped charges need to be liberated from dosimetric traps in order to obtain a readable signal. This means that the dosimeter can be read for a very short period of time and subsequently reread later with only a small correction made for depletion[38]. A relatively inexpensive and repeatable manufacturing process has been developed so commercially-available dosimeters have highly uniform sensitivity and properties[38]. Jursinic[10] has shown that sensitivity remains essentially unchanged up to accumulated doses up to 20 Gy, so Al_2O_3:C dosimeters can be reliably bleached and reused up to this threshold. A relative disadvantage of Al_2O_3:C is its effective atomic number of 11.28[44], which makes it oversensitive to low-energy radiation[34].

The reusability and rereadability of Al_2O_3:C OSL dosimeters are considerable advantages over standard LiF TLDs[29]. In addition, OSLDs do not require temperature and weight control as do TLDs, overall reading time is reduced, and the cost per reading is much lower. Furthermore, OSLDs are commercially available in a wide range of physical sizes and packages, including the planar style used in this work.

1.3. Hypothesis and Specific Aims

1.3.1. Hypothesis

The hypothesis of this work is that a *mailable, OSLD-compatible ^{192}Ir HDR brachytherapy phantom suitable for RPC monitoring of clinical trial sites can be developed with the ability to measure HDR dose accurately to within ±5%.*

1.3.2. Specific Aims

In order to test the hypothesis, this project has three specific aims:

1) Design and construct a phantom prototype – In order to be a useful remote audit tool, the phantom must be physically durable and reasonably sized so that it can be reliably mailed to participating institutions. It shall be simple and intuitive in design such that any instructions included in the program will be easily understood and implemented by participating physicists. It shall also be designed for use with commercially-available nanoDot OSL dosimeters, for which the RPC already has substantial infrastructure and expertise. And finally, its attenuation and scattering properties shall be as similar as possible to that of water for gamma rays in the ^{192}Ir energy spectrum in order to minimize deviations from the conditions specified in the TG-43 protocol.

2) Characterize the OSLD + phantom system – All the properties of dosimeters irradiated in the phantom as well as the phantom's physical properties must be well known in order to achieve overall system accuracy. Correction factors for dosimeter signal fading over time, reading linearity with delivered dose, and dose-rate dependence must be calculated. A phantom correction factor must be determined to convert results from in-phantom measurements to the TG-43 standard. The effects of variations in source and OSLD positioning within the phantom must be understood.

3) Determine the measurement accuracy of the system and demonstrate feasibility as a remote audit tool – The system must be able to measure dose with accuracy suitable for monitoring of clinical trial sites. The uncertainty in measured doses must be known. This uncertainty must be low enough such that a ±5% acceptance criterion – matching that of the RPC's external beam audit program – may be established for the HDR audit program as well. The system must be an accurate, practical, and easy-to-use tool when sent to outside institutions to audit HDR brachytherapy source strength and planning workflows.

2. Methods and Materials

2.1. Phantom Prototype

The phantom prototype was designed with the goals of a remote audit program in mind. The logistics of a mailable system make it infeasible to scale the phantom to a size sufficient for full scatter conditions, which Pérez-Calatayud *et al.*[45] estimated to be a sphere of radius 40 cm. Previous studies have investigated ^{192}Ir dosimetry in both spherical[45] and cylindrical[46] sizes ranging down to 10 cm radius, in both cases showing poor adherence to results obtained using an unbounded phantom. With the understanding that any phantom which accurately approximates the scatter conditions of an infinite phantom would necessarily be too large to form the basis of a mailed dosimetry program, it was decided that the prototype should be kept small and any effects resulting from the lack of full scatter accounted for in a block correction factor. However, the phantom should also be large enough so that the source and dosimeter(s) are at clinically-relevant distances from each other and at least some backscatter may be captured.

In terms of material, a solid phantom was preferable over a water-filled phantom as a requirement that participating institutions properly fill and drain a water phantom complicates instructions and might introduce extra uncertainties. Additionally, OSLD nanoDots are not waterproof and a water-filled phantom presents certain difficulties in loading, unloading, and protecting the dosimeters. However, a solid material that does not significantly perturb dose when compared to water for an ^{192}Ir energy spectrum is desirable as the TG-43 formalism for brachytherapy dosimetry requires the medium to be water or water-equivalent. Lastly, the material of the phantom must address the unique demands of a mailed program in that it should be physically durable, relatively inexpensive, and reasonably machinable.

It was decided that the phantom should have a single channel drilled into it to facilitate the insertion of a single tandem HDR source train. A single channel is preferable to a configuration with multiple HDR channels because it reduces complexity and the time required for planning and irradiation while also being sufficient to accurately audit source strength. The diameter of the channel was chosen so that it would admit a standard-size catheter of a type that any clinic providing common HDR clinical treatments should have on hand. A long channel length was chosen so that a plan with enough dwell positions to provide a flat isodose line in the region of the

dosimeter could be created. While a single dwell position might have reduced the time required for planning and irradiation, a curved isodose line across the profile of the dosimeter is undesirable as this may introduce extra uncertainty in the nanoDot reading and thus the dose measurement.

A phantom capable of holding multiple dosimeters was preferable to single-dosimeter designs. Having more than a single dosimeter in the phantom provides multiple independent measurements and, in certain arrangements, mitigates the effects of some types of positioning uncertainty. The distance between the dosimeters and the source should be on the order of clinically relevant distances. Lastly, the dosimeters must be positioned and the phantom designed such that the nanoDots are easy to load and remove, as it is expected that the phantoms will be reused constantly as part of an RPC audit program.

2.2. OSL Dosimeters

2.2.1. nanoDots

This study and the proposed remote audit program both utilize a specific Al_2O_3:C OSLD packaging offered by Landauer under the nanoDot brand name (Landauer , Inc., Glenwood, IL) and shown in Figure 2.1. NanoDots have been used by the RPC for its external beam audit program with tremendous success[4]. Overall single standard deviation uncertainty of external beam dose measurements using nanoDot OSLDs in the RPC's program has been calculated as 1.8%[7]. The RPC already has considerable expertise and infrastructure in place for the deployment of nanoDot dosimeters, with more than 10,000 individual dosimeters in circulation as part of the external beam program as of 2012. NanoDots have been shown to be unaffected in any significant way by reasonable temperature and humidity changes encountered during the mailing process[5].

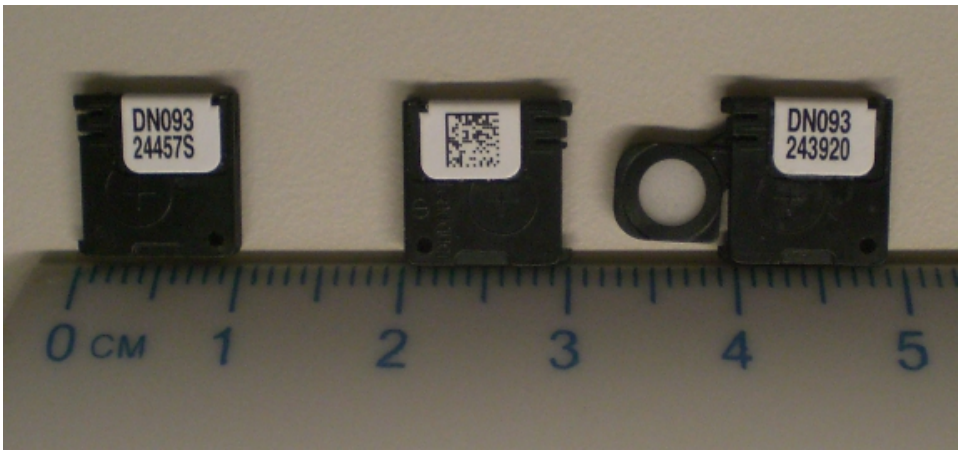

Figure 2.1: Examples of the nanoDot OSL dosimeters used in this work. From left to right: nanoDot front showing label with unique identification number, nanoDot back showing unique barcode, and nanoDot with active dosimeter (white circular area) pushed out of cassette and exposed.

Each nanoDot consists of a light-tight plastic cassette with a slide-out tray that holds a small disc of active dosimeter material. The external dimensions of the cassette are 10 × 10 × 2 mm^3. The disc of dosimeter material is 5 mm in diameter and may be considered nearly planar, with a thickness of approximately 0.3 mm (see Figure 2.2). During the manufacturing process, batches of Al_2O_3:C powder are mixed with an organic binding agent and printed on a tape of plastic substrate. Discs are then punched from the tape for use as individual dosimeters. This mixing process ensures that all of the Al_2O_3:C powder has the same sensitivity and properties, however differences in the amount of OSL powder deposited on each disc means that the characteristics of individual dosimeters may vary.

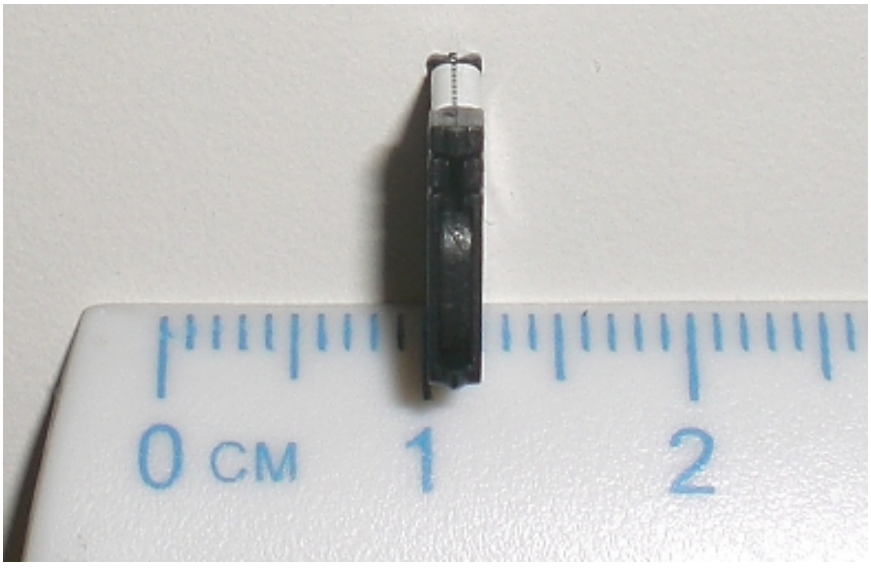

Figure 2.2: An OSLD nanoDot cassette, pictured edge-on to show its 2 mm thickness. The active dosimeter inside the cassette is approximately 0.3 mm thick.

An important property of nanoDots and all Al_2O_3:C material in general is reusability. Jursinic[10] found sensitivity unchanged up to a cumulative dose of 20 Gy, but the RPC uses 10 Gy as a threshold and that cumulative dose was not exceeded for any individual dosimeter used in this work. Between irradiations, each nanoDot was optically annealed for a minimum of 24 hours using a custom-built cabinet with four 54-watt fluorescent bulbs. Each lamp emits an average of 4700 lm at 4100 K. The lamps are fitted with a UV filter which blocks all light with a wavelength of less than 395 nm.

2.2.1.1. Element Correction Factor

Although the manufacturing process is designed to minimize variations within a single batch, some differences in the sensitivities of individual nanoDots are inevitable. These may be due to random fluctuations, differences in the amount of Al_2O_3 deposited on each dosimeter, or even slight amounts of damage that may occur before the nanoDot is commissioned. In order to ensure consistency in measurements made with different dosimeters, an Element Correction Factor (ECF) is calculated for each individual dosimeter. To determine ECFs, a large sample of dosimeters from each batch is irradiated with a ^{60}Co source under controlled conditions to a known low dose (approximately 25 cGy). Then, each individual dosimeter is read and its raw reading compared to the average raw reading of the entire sample of dosimeters. The ratio of these readings is the Element Correction Factor. ECFs for individual dosimeters can deviate from unity by more than ±9%. Every time a dosimeter is read, its average raw reading is multiplied by that nanoDot's unique ECF in order to correct for variations in the nanoDot sensitivity throughout the entire batch of dosimeters.

2.2.2. OSLD Reading

2.2.2.1. MicroStar Reader

Landauer's microStar reader (Landauer, Inc., Glenwood, IL), shown in Figure 2.3, is used for reading nanoDot dosimeters. The reader features a light-tight chamber into which a single nanoDot may be inserted via a pull-out tray. Inside the chamber is an array of 36 LEDs and a photomultiplier tube. After a nanoDot is placed in the chamber and the reading procedure initiated, a mechanism inside the reader pushes the dosimeter disc out of the nanoDot cassette and turns on the LED array. Light from the array stimulates emission from the dosimeter material, which is collected by

the photomultiplier tube. This process is known as continuous-wave OSL, or CW-OSL. The microStar reader interfaces with a personal computer so that readings may be easily recorded.

Figure 2.3: The microStar OSLD reader with tray pulled out. NanoDot OSLDs are read by inserting a single dosimeter into the black adapter jig pictured, then inserting the jig into the tray. The tray is pushed in and the knob turned to initiate the reading process.

The light emitted by the LED array for stimulation must not interfere with the light released as a result of stimulation, or else the reading results will be highly inaccurate. To account for this, the reader has two optical bandpass filters. The first filter, a Schott OG515, filters light emitted by the LEDs. The LED-filter combination has a peak emission at 540 nm[10]. A second filter, a Hoya B-370, is placed in front of the photomultiplier, and the PMT-filter combination has peak sensitivity at 420 nm[10]. This matches the dominant emission band of Al_2O_3:C arising from F-center luminescence.

2.2.2.2. Standards and Controls

Prior to each reading session, certain nanoDots known as “standards” are irradiated to an accurately-measured dose close to 100 cGy under carefully controlled conditions. The standards are placed in a custom acrylic miniphantom which is placed in a ^{60}Co beam with a 10 × 10 cm^2 field size.

The SSD to the top of the platform is 80 cm and the standard OSLDs are at the midpoint of the 1.5 cm thick phantom, meaning that source-to-dosimeter distance is 79.25 cm. The timer end effect of the ^{60}Co unit console is 0.01 min and is accounted for in the irradiation of the standards. The actual dose delivered to each standard is determined with the formula:

$$Dose = Output \times e^{\left(\frac{-\ln 2 \times d}{365.25 \times 5.26}\right)} \times (time + end\ effect) \quad (2.1)$$

where *Output* is the machine output at calibration in cGy/min, *d* is the number of days elapsed from calibration to irradiation, *time* is the console-reported beam on time in minutes, and *end effect* is 0.01 min for all irradiations to account for source transit time. The half life of ^{60}Co is 5.26 years. The irradiation of all standards was performed on the Cobalt V2 unit at M.D. Anderson Cancer Center, which was calibrated on October 15, 2005 and found to have an output of 147.90 cGy/min at 79.25 cm. At the start of each reading session, a standard is read. A separate standard is read at the end of the session. The average reading from the two standards is used to establish the reading system's sensitivity (that is, dose per raw reading) which will be discussed in detail below.

Also read during an OSLD reading session are nanoDots known as "controls". Controls are irradiated under very similar conditions to standards, with the main difference being that controls are irradiated in groups of up to 30 at a time using a special rotating jig. The jig rotates at 10 rpm while the controls are under irradiation, to ensure uniform dose to all of the dosimeters. The dose delivered to the controls is approximately 90 cGy, compared to approximately 100 cGy delivered to standards. All controls were irradiated on the Cobalt C unit at M.D. Anderson Cancer Center, which was calibrated on October 15, 2005 with an inverse-square corrected output of 84.73 cGy/min. Actual dose was calculated for controls using Equation 2.1, with the only difference being that *end effect* = -0.01 min for the Cobalt C unit.

Controls are read at the beginning and end of a session along with standards, as well as in the middle of a session if many (more than a dozen or so) experimental dosimeters are being read during the session. The purpose of reading controls is to identify any substantial drift which may occur in the sensitivity of the OSLD reader over the course of a reading session. If the drift direction of the controls differs from that of the standards, or if either drifts in excess of ±1.5% over the course of a session, consideration may be given to rereading the dosimeters or establishing a linear correction factor to account for the drift.

2.2.2.3. Reading Procedure

Before reading any dosimeters, the microStar reader is allowed to warm up for a period of at least 30 minutes. A series of constancy checks are then performed on the reader. The number of counts acquired by the PMT with the LED array off during a certain time period, known as dark counts, is recorded. Then, the number of counts collected by the PMT when exposed to an internal ^{14}C source, known as PMT counts, is recorded. Finally, LED counts, which is the number of counts collected by the PMT while the LED array is switched on, is collected. Dark counts, PMT counts, and LED counts are measured a minimum of three times each and the three readings are compared and the overall averages compared to tests from previous sessions to verify that the reader is functioning properly.

After constancy checks are completed, one standard and one control dosimeter are read as outlined above. Then, reading of experimental OSLDs commences. To read an OSLD, the barcode on the nanoDot is scanned for record-keeping purposes. Then, the nanoDot is fitted into a specially-designed holder and placed in the reader's tray. The tray is slid into the reader, which is light-tight. Turning a knob on the reader's face slides the dosimeter material out of the nanoDot cassette and turns on the LED array. The dosimeter is stimulated for a period of 7 seconds after which the LED array turns off and the knob is turned back to its home position, which returns the dosimeter disc to the light-tight nanoDot cassette. While the dosimeter is being stimulated, the PMT integrates all incident photon counts and the system reports this number once the 7-second reading is complete.

The reading process is repeated in its entirety three times for each dosimeter. Subsequent readings of an OSLD cause a measureable depletion of the emitted OSL signal. The RPC has developed an empirical depletion correction factor (*DCF*) to account for this phenomenon:

$$DCF = \frac{1}{(-5.148 \times 10^{-6}) \cdot n^2 + (-1.277 \times 10^{-3}) \cdot n + 1} \qquad n = 0,1,2 \ldots \tag{2.2}$$

where *n* is the reading number. All raw OSLD readings in this experiment were corrected with this factor. A control nanoDot is often read near the middle of the session as mentioned above. Lastly, one control and then one standard are read at the end of the session, after all experimental OSLDs have been read.

2.3. HDR Sources

2.3.1. Nucletron MicroSelectron v2

For the majority of irradiations performed in this work, a microSelectron-HDR afterloader (Nucletron, Columbia, MD) (shown in Figure 2.6) and microSelectron-HDR "version 2" ^{192}Ir source (Nucletron model number 105.002, Nucletron, Columbia, MD) housed at the University of Texas M.D. Anderson Cancer Center were used. Daskalov *et al.*[47] described this source in detail and a schematic drawing is shown in Figure 2.4. The design, introduced in 1998, consists of a cylinder of pure iridium metal 0.65 mm in diameter and 3.6 mm long. The radioactive ^{192}Ir is distributed uniformly throughout the iridium core. The source is encapsulated by 0.125 mm of AISI 316L stainless steel (68% Fe, 17% Cr, 12% Ni, 2% Mn, and 1% Si by weight, density = 8.02 g/cm^3), giving a total source and encapsulation diameter of 0.90 mm. The encapsulated source is welded to the end of a woven steel cable with diameter 0.7 mm. M.D. Anderson policy dictates that the ^{192}Ir sources are replaced approximately every four months with each new source having an activity at installation of approximately 10 Ci. The microSelectron-HDR afterloader has 18 channels and a cable length of 1500 mm. Oncentra TCS software version 3.1.3.800 (Nucletron, Columbia, MD) was used to control the afterloader and source.

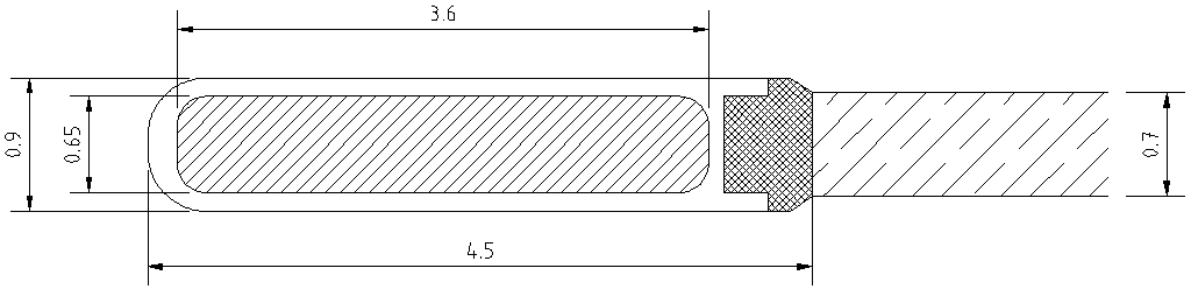

Figure 2.4: The Nucletron microSelectron-v2 HDR source in detail. All dimensions are in mm.

Prior to irradiating any dosimeters, source positioning accuracy was confirmed to within ±1 mm by irradiating a strip of radiochromic film marked in 1 mm increments supplied by the source manufacturer (see Figure 2.5). Next, a source calibration was performed to verify the institution's existing calibration. A Precision Radiation Measurement HDRC-1 well-type ionization chamber, serial number 9117, was used for the calibration. The well chamber was connected to a Standard Imaging MAX-4000 electrometer, serial number E061502. A 6 French endobronchial catheter was attached to channel 1 of the afterloader and the other end inserted into the well chamber. The source was stepped through 7 dwell positions at 0.5 cm increments. At each position, the current

reading of the electrometer was allowed to stabilize for a few seconds and then recorded. This process was repeated three times to give three current readings at each of the seven positions inside the well chamber. All three measurements were averaged together and the position corresponding to the highest average current selected as the point of maximum sensitivity of the well chamber.

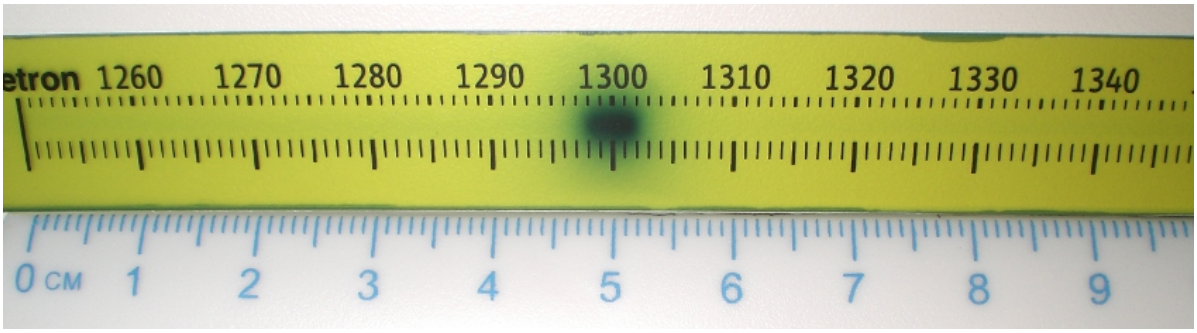

Figure 2.5: The radiochromic film used to verify the afterloader's source positioning accuracy prior to irradiation. If the source is positioned correctly, the center of the darkened spot on the radiochromic film should be at exactly 1300 mm.

Once the maximum current was measured in the well chamber, the formalism of DeWerd and Thomadsen[48] was used to calculate the air-kerma strength of the source:

$$S_K = I \times P_{elec} \times C_{T,P} \times N_{RK} \times A_{ion} \times P_{ion} \tag{2.3}$$

where S_K is the air-kerma strength of the source, I is the measured current, P_{elec} is the electrometer scale correction factor, $C_{T,P}$ is a correction for ambient temperature and pressure, N_{RK} is the ADCL-provided calibration factor for the well chamber, A_{ion} is the ADCL-provided correction for collection efficiency, and P_{ion} is the correction for collection efficiency at the time of measurement. The ADCL calibration report for the well chamber provided A_{ion} = 0.994 and the RPC has already determined the relationship between P_{ion} and source strength for the particular well chamber used. For the purposes of these calculations, P_{ion} = 1.005 was used. $C_{T,P}$ was calculated from measurements made at the time of calibration using the following equation:

$$C_{T,P} = \frac{273.2 + T}{295.2} \times \frac{760}{P} \tag{2.4}$$

where T is the temperature inside the well chamber during calibration in degrees Celsius and P is the atmospheric pressure in mm Hg. P_{elec} and N_{RK} were provided by the ADCL calibration reports for the electrometer and well chamber, respectively. These values were P_{elec} = 1.000 × 10^{-9} A/rdg and N_{RK} = 3.859 × 10^{11} U/A (where 1 U = 1 $\frac{\mu Gy \cdot m^2}{h}$).

Figure 2.6: The Nucletron microSelectron-HDR afterloader at M.D. Anderson Cancer Center.

The maximum average current recorded in the well chamber during calibration was 55.377 nA. Using Equation 2.3 and this current reading, an air-kerma strength of 21549 U was calculated. At the time of calibration, the treatment control system software reported an air-kerma strength of 21336 U. Thus, the calculated source strength differed from the machine-reported strength by approximately 1%. The measured air-kerma strength was used for all subsequent calculations and irradiations. A new calibration was performed using the same methods each time the source was replaced. Reports of each calibration performed are available in Appendix 6.2.

2.3.2. Varian VariSource VS2000

Additional dosimeter irradiations were performed on a Varian VariSource iX afterloader (Varian Medical Systems, Palo Alto, CA) and Varian Model VS2000 ^{192}Ir source (Varian Medical Systems, Palo Alto, CA) housed at The Methodist Hospital in Houston, TX. This source, introduced in 2000, has been described by Angelopoulos *et al.*[49] A schematic drawing is shown in Figure 2.7. The VS2000 source and the Nucletron source described above make up the large majority of the ^{192}Ir sources in clinical use for HDR brachytherapy in the United States today. A single VS2000 source

consists of two 2.5 mm long, 0.34 mm diameter cylindrical seeds of pure iridium. The radioactive ^{192}Ir is distributed evenly in each of the seeds. The seeds are adjacent to one another in tandem and encapsulated at the end of a metal wire. The wire is 0.59 mm in diameter giving an encapsulation thickness of 0.125 mm surrounding the Iridium. The composition of the wire is 55.6% Ni and 44.4% Ti by weight (density = 6.5 g/cm^3). It is notable that the physical geometry of the sources and the composition of the encapsulation differ between the Varian and Nucletron sources.

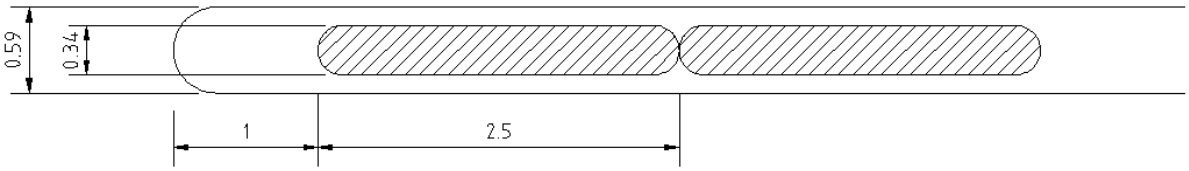

Figure 2.7: The Varian VS2000 source in detail. All dimensions are in mm.

The Varian source was calibrated on March 23, 2012 using the same procedures and equipment as were used to calibrate the Nucletron source. The maximum average current produced in the well chamber was 47.172 nA. Using Equation 2.3, this gives an air-kerma strength at calibration of 17961 U. Using the RPC's ^{192}Ir air-kerma-to-activity conversion factor of 4028 U/Ci gives a nominal activity for the Varian source of 4.459 Ci at calibration. At the time of irradiation, the Varian console reported a nominal activity of 4.454 Ci. The difference between the measured and reported activities is thus approximately 0.1%. Again the measured air-kerma strength was used as the gold standard for all calculations involving the Varian source. The calibration report may be found in Appendix 6.2.

2.3.3. Treatment Plan

For the irradiations in this study, a simple HDR treatment plan – hereafter known as the "standard plan" – was created using BrachyVision version 8.9.15 (Varian Medical Systems, Palo Alto, CA). As do all HDR brachytherapy planning systems in common clinical use at this time in the United States, BrachyVision uses the methodology and assumptions of AAPM Task Group 43[19]. The BrachyVision installation used to create the standard plan was commissioned using the ^{192}Ir TG-43 parameters published by Daskalov *et al.*[47] for the Nucletron source.

The standard plan uses 10 dwell positions, spaced 5 mm apart, in a single tandem applicator. A dose of 100 cGy in a single fraction was prescribed to two reference lines parallel to the applicator and 2 cm away laterally. The treatment planning software was instructed to calculate

dwell times individually for each source position with the two reference line objectives weighted equally. The software was allowed to optimize for 5 minutes. The source strength in the system was set to 40300 U, which for ^{192}Ir corresponds roughly to a 10 Ci source. The isodose lines for the standard plan are shown in Figure 2.8.

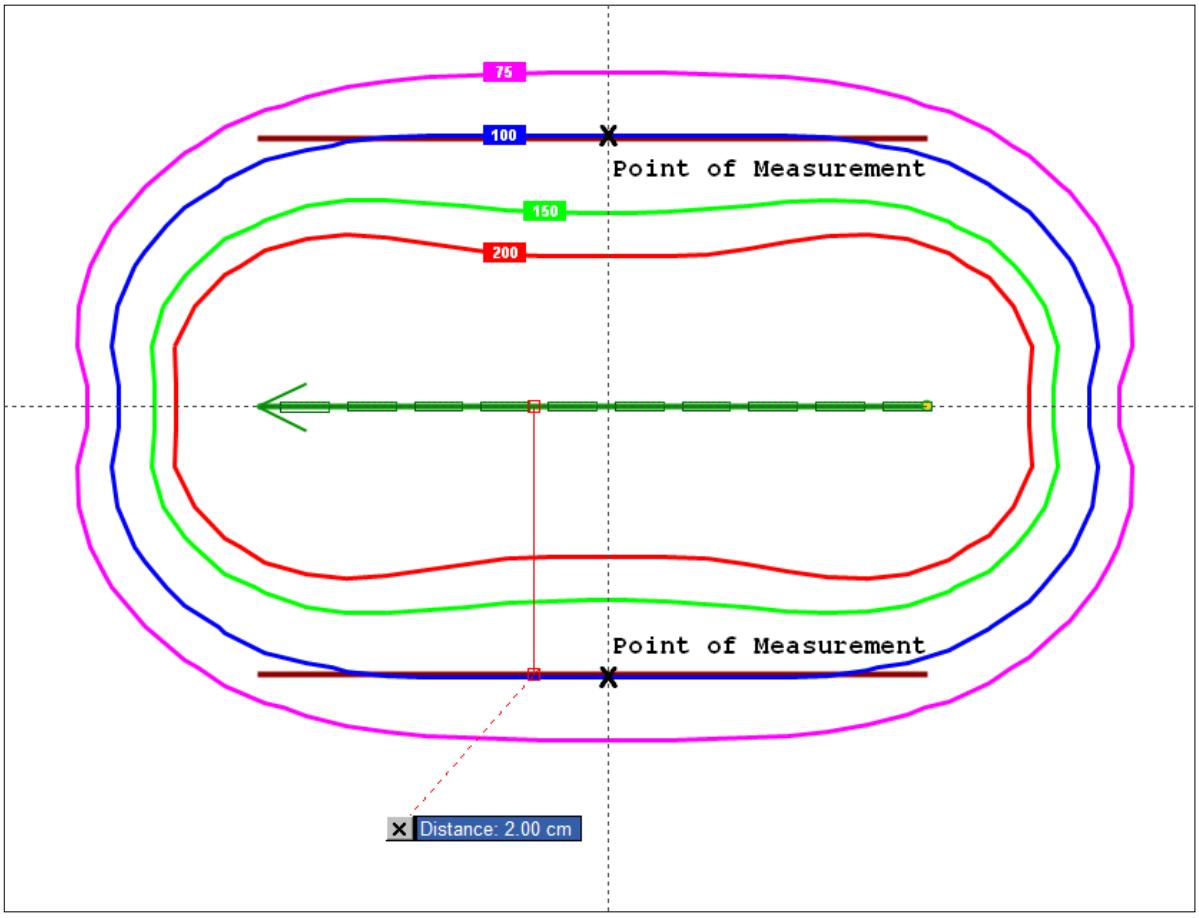

Figure 2.8: The isodose lines of the "standard plan". Doses are in cGy.

After optimization, the point dose reported by BrachyVision at a point 2 cm away from the central channel laterally and on a line bisecting the source train was recorded. This point corresponds to the center of the dosimeter slot in the phantom and is regarded as the point of measurement. The actual dose reported by BrachyVision at this point was 100.6 cGy, and this number was subsequently used as the actual dose delivered to the point of measurement for all irradiations using the standard plan. To obtain the dose at the point of measurement for the same plan using the Varian VS2000 source, TG-43 calculations were used since BrachyVision had not been commissioned for use with that source. For these calculations, the TG-43 parameters published by Taylor and Rogers[50] for the Varian source were used. The result of TG-43 calculation was a dose of

101.76 cGy at the point of measurement and this was likewise used as the actual dose delivered by the standard plan when irradiating with a Varian source.

The standard plan was used as a basis for all irradiations performed in this study by scaling the dwell times. Depending on the current source strength, new dwell times were calculated to deliver the desired dose to the point of measurement using the following relationship:

$$t'_n = \left(\frac{40300\ U}{SS}\right) \times \left(\frac{desired\ dose}{standard\ dose}\right) \times t_n \quad n = 1 \ldots 10 \tag{2.5}$$

where *SS* is the current source strength in U, *desired dose* is the desired dose in cGy, t_n is the standard plan's dwell time for position *n*, and t'_n is the new dwell time for position *n*. *Standard dose* is the dose delivered to the point of measurement using the unmodified standard plan and a source strength of 40300 U; it is equal to 100.6 cGy for Nucletron sources and 101.76 cGy for Varian sources as detailed above.

2.4. OSL Dose Calculations

2.4.1. Dose Calculation Equation

The equation to calculate dose from an OSL reading is as follows:

$$Dose = (avg.corrected\ rdg.) \times ECF \times Sensitivity \times K_F \times K_L \times K_B \tag{2.6}$$

where *average corrected reading* is the average of the three depletion-corrected independent readings of the dosimeter, *ECF* is the element correction factor as discussed above, *Sensitivity* is the system sensitivity for the reading session, K_F is the fading correction factor, K_L is the linearity correction factor, and K_B is the block correction factor which is unique to the phantom used in this work.

The average corrected reading is the average PMT counts from three separate readings of the same dosimeter. The second and third readings are corrected individually using Equation 2.2. If the percent standard deviation of the three depletion-corrected readings was greater than 0.8%, the individual reading for that particular dosimeter which was inconsistent with the others was not used. If the deviation among the three readings was acceptable, the readings were averaged and the result became the average corrected reading for that dosimeter.

In practice, dose is always calculated on the basis of the average calculation from two dosimeters irradiated at the same time in the phantom. This greatly reduces uncertainty due to relative source positioning (see Section 4.5.2.). The cylindrical symmetry of any single-channel tandem HDR treatment plan ensures that the only variation in the dose delivered to the phantom's two dosimeter slots will be due to lateral variations in source positioning. The intended use of the phantom calls for always loading two dosimeters and averaging their measurements, and all statistics and results quoted in this work are based on that assumption. In general, the word "measurement" will be used here to indicate the average from two dosimeters irradiated at the same time, and any discussion of individual dosimeter readings will be clearly specified.

2.4.2. System Sensitivity

System sensitivity is determined anew for each OSLD reading session. In order to determine sensitivity, one standard dosimeter is read at the beginning of the session, and a separate standard read at the end of the session. Each standard is read three times and depletion corrected using Equation 2.2 as are all OSLD readings. Then, system sensitivity is calculated using the following formula:

$$System\ Sensitivity = \frac{Expected\ Dose\ to\ Standard}{avg(avg.corrected\ reading) \times K_F^{std} \times K_L^{std}} \tag{2.7}$$

where *Expected Dose to Standard* is the actual dose delivered to the standards as calculated by Equation 2.1. *Average(average corrected reading)* is the average of the two depletion-corrected standards readings, one at each end of the session. K_F^{std} is the fading correction factor for the two standards read (two standards irradiated on the same day, and thus to the same dose, are always used), and K_L^{std} is the linearity correction factor for the standards. For the batch of nanoDot dosimeters used in this work, K_L^{std} has already been established by the RPC:

$$K_L^{std} = (-1.374 \times 10^{-4} \times raw\ dose) + 1.013 \tag{2.8}$$

where *raw dose* is the dose delivered to the standard in cGy as determined by Equation 2.1. This is the linearity correction factor currently in use for all standards coming from the batch of dosimeters used in this work and shall not be redetermined here. It should be noted that in practice, $K_L^{std} \approx 1$ in general in this experiment, since the only standards used were those irradiated to approximately 100 cGy.

2.4.3. Fading Correction Factor

Previous experiments at the RPC[4] have already determined the fading correction factor for the batch of nanoDot dosimeters used in this experiment. Dosimeters were irradiated to identical doses on different days ranging from 1 to 120 days prior to reading and all were read at the same time. The relationship between OSL signal and days after irradiation can be described thusly:

$$K_F = \frac{1}{1.005 \times d^{-0.0072}} \tag{2.9}$$

where *d* is the number of days since irradiation. This is the correction factor used to correct for fading for every standard, control, and experimental dosimeter used in this study.

No dosimeter in this study was read before at least 5 days had elapsed since irradiation. This is to allow the response to decay into the flatter and more stable part of the fading curve prior to reading.

2.4.4. Linearity Correction Factor

The literature has shown that Al_2O_3:C sensitivity is dependent on dose[10, 51]. However, previous determinations of the extent of this dependency typically investigated higher energy radiation than the ^{192}Ir spectrum and used experimental setups substantially different from the phantom prototype presented here. For example, the RPC's own K_L^{std} was determined from irradiations of OSLDs placed in a custom acrylic miniphantom using a ^{60}Co source. As a result, it was determined that dose response should be investigated anew using the setup specific to this work and a unique linearity correction factor, K_L, determined for use with the system described here.

Three independent sets of irradiations were used to determine the linearity correction factor of the system. Prior to each set, Equation 2.5 was used to calculate dwell times necessary to deliver nominal doses ranging from 50.3 (100.6 ÷ 2) cGy to 402.4 (100.6 × 4) cGy where 100.6 cGy is the dose at the point of measurement under the standard plan with a Nucletron source. Each set of irradiations was performed in less than one hour, so no correction for the decay of the source during irradiation was made (the decay in source strength over a time of one hour is less than 0.04%). The number of individual dosimeters irradiated at each dose level is shown in Table 2.1.

Table 2.1: Number of individual dosimeters irradiated to specific doses for each of three linearity trials.

Trial #	Dose						Total
	50	75	100	200	300	400	
1	4	0	10	4	4	4	26
2	4	0	8	4	4	4	24
3	0	8	8	6	6	0	28
Total	**8**	**8**	**26**	**14**	**14**	**8**	**78**

Each dosimeter was read and depletion corrected, and the ECF applied. Then, the nominal dose was divided by the corrected average counts for each dosimeter to obtain a quantity called dose response $\left(dose\ response = \frac{nominal\ dose}{corrected\ avg\ counts}\right)$. In this case, nominal dose was the intended dose delivered to the dosimeter as used in Equation 2.5 to calculate dwell times. The dose response value for each dosimeter was then plotted versus the nominal dose. A linear regression was applied to obtain a relationship between dose response and nominal dose. After the fit was obtained, the line was normalized to the predicted dose response value at 100 cGy. This normalized dose-response-versus-nominal-dose curve is known as K_L and it is important to note that $K_L \equiv 1.000$ at 100 cGy.

The K_L lines calculated individually from each of the three data sets were in good agreement so the data were combined for the overall final K_L determination. The same process was applied to the combined data set as was used for the individual data sets. Thus, the final K_L line calculated is in effect an average of the three linearity trials which have been weighted by the number of dosimeters used for each trial.

2.4.5. Block Correction Factor

The block correction factor (also known as the energy correction factor) is unique to the OSLD dose calculations performed in this work. Because this project aims to produce a mailable and OSLD-compatible phantom, a small plastic phantom is much more practical than a spherical water phantom with a radius of perhaps 30 cm. Therefore the block correction factor, K_B, is necessary to convert the quantity measured by this experiment, which is dose to polystyrene in a specific phantom geometry, to the standard for brachytherapy dosimetry as dictated by TG-43, which is dose to water in a large water phantom.

Both the physical density of high-impact polystyrene (ρ = 1.04 g/cm^3) and the mean atomic number[52] (Z = 5.29, 92.3% C and 7.7% H by weight) differ from that of water (ρ = 1.00 g/cm^3, Z =

6.60, 88.8% O and 11.2% H by weight). However, Meli *et al.*[53] found the photon energy spectrum of an ^{192}Ir source in polystyrene to be "essentially identical" to that of water at depths of 1, 5, and 10 cm. On the other hand, Pérez-Calatayud *et al*.[45] found that the radial dose function of an ^{192}Ir source in a small (r = 10 cm) spherical polystyrene phantom falls off very quickly in moving away from the center when compared to that of an unbounded water phantom. This is due to the loss of dose due to scattered photons in the smaller phantom. Dose lost due to lack of full scatter conditions is constant and thus may be corrected for.

The nanoDot dosimeters used in this work also have some angular dependence. Kerns *et al.*[54] found approximately 2% lower response in nanoDots irradiated at a 45° angle, increasing to almost 4% lower at 90°, using a 6 MV photon beam. This is relevant because the end positions in the source train of the standard plan used in this study, which have the longest dwell times and contribute the most to the dose at the point of measurement, are at an angle of approximately 42° from the dosimeter. However, since the geometry of the source and dosimeter setup cannot change, a correction factor to account for any angular dependence effect is appropriate.

Lastly, and most importantly, Al_2O_3:C is known to over-respond at energies lower than the 662 keV gamma emission of ^{137}Cs due to its relatively high effective atomic number and density[33]. Jursinic[10] found a 6% increase in the sensitivity of Al_2O_3:C OSL dosimeters under ^{192}Ir irradiation when compared to 6 MV x-rays. Since the RPC uses ^{60}Co (average energy = 1.25 MeV) to irradiate the standard OSLDs which ultimately determine system sensitivity (as discussed above), the increased sensitivity of OSL material to the ^{192}Ir energy spectrum must be accounted for. However, since the phantom in this project is designed and intended for ^{192}Ir HDR sources and will only be used for the dosimetry of that isotope, a constant energy correction factor may be determined and applied. This correction factor can at the same time account for potential angular dependence effects and loss of signal due to lack of full scatter conditions. All of these corrections combined into a single term are what we refer to as the block correction factor, K_B.

In order to determine K_B, 20 measurements were made during a single session using a Nucletron source. Each dosimeter was irradiated to the same dose using identical dwell times. The entire irradiation session was completed in less than one hour, during which the ^{192}Ir source is calculated to have decayed less than 0.04% so no attempt to correct for source decay during the session was made. The dosimeters were read and the raw readings recorded. Then, rearranging Equation 2.6 gives an expression for K_B:

$$K_B = \frac{Dose}{(avg.corrected\ rdg.) \times ECF \times Sensitivity \times K_F \times K_L} \quad (2.10)$$

In this equation, *Dose* refers to the expected dose at the point of measurement using the standard plan as reported by the treatment planning system. The linearity correction factor K_L is also based on the expected dose. All other terms are as previously explained.

For each of the 20 measurements, the quantity $[(avg.corrected\ rdg.) \times ECF \times Sensitivity \times K_F \times K_L]$ – the denominator in Equation 2.10 – was calculated. This quantity is the fading- and linearity-corrected dose to polystyrene in the phantom geometry. This dose is also based on the assumption of irradiation under a ^{60}Co-equivalent spectrum, as the *Sensitivity* calculation at the time of OSLD reading is referenced to that spectrum. However, ideally the *Dose* calculated from Equation 2.6 would be the dose to water in a large phantom with sensitivity referenced to the ^{192}Ir energy spectrum. Converting the in-phantom *Dose* to one following these assumptions and conditions would allow for direct comparison between doses as measured by OSLDs in the phantom and doses calculated by TG-43, which is the algorithm most commonly used by commercially-available treatment planning systems. Thus, from Equation 2.10 we know that K_B must have units of $\frac{[Dose]_{H_2O}^{Ir-192}}{[Dose]_{phantom}^{Co-60}}$, that is, dose to water in a large phantom (i.e., TG-43 stipulations) from an ^{192}Ir source divided by dose to polystyrene in the HDR phantom geometry from a ^{60}Co source. By measuring a block correction factor with these units, the final result of Equation 2.6 is a measurement of TG-43-consistent dose to water under ^{192}Ir irradiation, a quantity comparable to that provided by commercial HDR planning systems.

After a K_B value was calculated individually from each of the 20 measurements, the values were averaged to give the average overall system K_B. It was discovered during preliminary calculations that the average K_B calculated based on irradiations with a Nucletron source gave unacceptably inaccurate results for irradiations performed with the Varian source. For a sample of 10 measurements made with a Varian source, the doses calculated from OSLD readings using $K_B^{Nucletron}$ were approximately 2% higher than the expected doses determined from TG-43 calculations. None of the ten measurements produced a value below the expected dose. The reasons for this difference are discussed in Section 4.2.

To improve measurement accuracy, a set of 10 additional measurements were made using a Varian source in the same way as those made with the Nucletron source. K_B was calculated

independently for Varian measurements and that value used for all subsequent experiments involving the Varian source. The result is two different block correction factors, $K_B^{Nucletron}$ and K_B^{Varian}, and it is expected that the same process would need to be repeated for any new ^{192}Ir sources introduced into clinical use whose geometry differs considerably from that of the Nucletron and Varian sources used in this study.

2.4.6. Dose Rate Effect

A new source was installed in one of the clinical HDR afterloaders at M.D. Anderson Cancer Center on April 11, 2012. The source was calibrated following the procedure in Section 2.3.1. On April 12, 2012, with the air-kerma strength at 45336 U, a single measurement was made with the dwell times chosen using Equation 2.5 to deliver a dose of 100.6 cGy. This process was repeated a total of eight times at irregular intervals over the next three months as the source strength decayed. Each time, the dwell times were recalculated using the current source strength and Equation 2.5 to deliver a nominal dose of exactly 100.6 cGy. Thus it is possible to compare the actual doses measured after delivering the same nominal dose using the full range of clinically-relevant source strengths. Any significant trend among the measured dose data would indicate a dose-rate dependence in the dosimeters.

2.5. Phantom Characterization

Once K_L, K_B, and potential dose rate effects have been established, the ability to make accurate measurements of dose using the phantom is complete, as all terms in Equation 2.6 are now known. Dose measurements were subsequently used to investigate certain physical properties of the phantom/OSLD system itself. Among these are the effect of the orientation of the OSL dosimeters in the phantom slots, and the effect of the distal/proximal positioning of the source train within the channel.

2.5.1. OSLD Orientation

In order to ensure that careless placement of dosimeters in the phantom slots would not significantly affect the system's accuracy, measurements made with OSLDs inserted into the phantom in various orientations were compared. Each nanoDot dosimeter has a paper label affixed to the outer cassette with unique identifying numbers printed on it. The label is in the same location and orientation on each nanoDot. The typical orientation when placing dosimeters in the

phantom was with the numbers facing “in” and “up”; this orientation was used in all other irradiations performed in this work for both Nucletron and Varian sources. In terms of orientation, “in” was defined as the label facing the phantom channel and HDR source, and “up” was the orientation having the label in position to be exposed to the air when the sections of the phantom were pulled apart. We define “out” and “down” as opposite of “in” and “up”, respectively. Figure 2.9 shows a “source’s-eye view” of the eight possible OSLD orientations along with the terms used to define them.

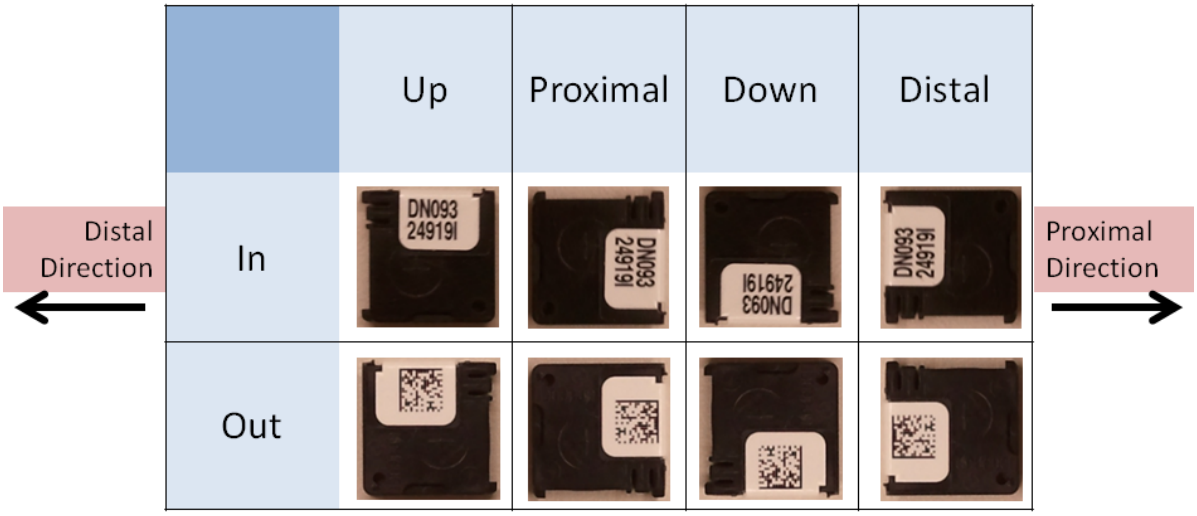

Figure 2.9: Source's-eye view of the eight possible OSLD orientations.

Two dosimeters were placed in the phantom in the standard (in and up) orientation and irradiated to a nominal dose of 50.7 cGy. Then, two new dosimeters were inserted, but rotated 90° such that the labels of both were oriented toward the proximal direction of the source wire. These dosimeters were irradiated to the same dose. This process was repeated with two more dosimeters each with the labels oriented down, and then again with the labels oriented distally. The entire procedure was then repeated with dosimeters facing out and rotated through all four 90° orientations. The end result is 8 measurements – one at each orientation – covering the 8 possible orientations that a nanoDot could be inserted into the phantom.

2.5.2. Distal/Proximal Source Positioning

The isodose lines of the standard plan and the audit instructions to plan and deliver 100 cGy to a line (rather than a point) indicate that minor deviations in the distal/proximal positioning of the entire source train should have a minimal effect on dose measurements. In order to quantify this effect, measurements were made after moving the entire 10-position source train in discrete

steps away from the distal end of the phantom channel. All other irradiations in this work were carried out with the catheter inserted fully into the phantom channel and adjacent to the end of the channel and the source train occupying the 10 most distal dwell positions available.

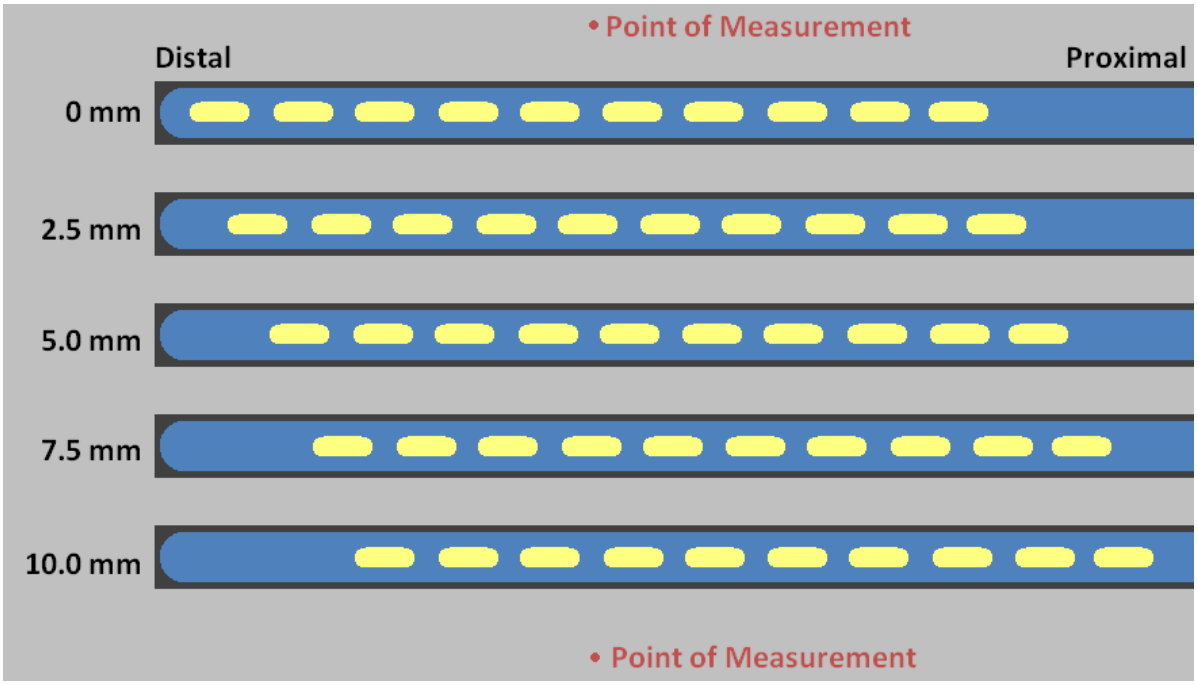

Figure 2.10: The test set up to measure the effect of distal/proximal positioning errors. For each test, the catheter (blue) is inserted fully into the channel (dark gray). The entire source train (10 individual sources in yellow) is shifted toward the proximal end of the catheter in 2.5 mm steps but otherwise remains the same. The point of measurement remains the same for all irradiations.

To investigate distal/proximal positioning, a catheter was inserted until it was adjacent to the end of the channel and then the standard plan delivered as usual but with one key deviation: the entire source train was shifted proximally inside the catheter a distance of 2.5 mm. This procedure was repeated with the source train shifted 5.0, 7.5, and 10.0 mm proximally. Figure 2.10 shows the entire source train being stepped back from the distal end of the catheter as the point of measurements remains the same.

2.6. Trial Remote Audits

After the phantom was characterized, several institutions which provide ^{192}Ir HDR brachytherapy were enlisted to test the system as a potential remote audit tool. Each institution was provided with the phantom preloaded with unirradiated OSLDs, instructions on how to set up, plan, and deliver 100 cGy to the dosimeters, and a form on which to record machine, source, and plan characteristics. During this evaluation period, a questionnaire to collect the participating

physicists' opinions on the system was also provided. The physicist contact at each institution was informed that the system was a potential new RPC remote audit program analogous to the current external beam audit programs but not provided with additional context or instructions beyond those provided by mail along with the phantom.

After the phantom and dosimeters were returned to the RPC, the dose was measured by reading the two OSLDs, converting the readings to dose with Equation 2.6, and averaging the two doses together to provide a single measurement. This quantity is known as the "RPC measured dose" or simply "RPC dose". The institution-reported dose at the point of measurement as determined by the institutional treatment planning system is known as the "institution dose". Additionally, each institution's self-reported source model, source strength, and dwell times were used to calculate the dose at the point of measurement using TG-43 formalism. This calculated quantity is hereafter known as the "TG43-calculated dose" or "TG-43 dose". For each remote audit these three quantities and the RPC/institution ratio, which is the quantity of most interest, were calculated. The institution dose was the quantity used as the nominal dose delivered to the dosimeters for the purposes of calculating the linearity correction factor. The institution's feedback on the program as reported on the questionnaire was recorded as well.

2.6.1. Instructions

The written instruction sheet mailed with the phantom during trial remote audits is shown in Appendix 6.3.1. The instructions include steps on how to set up the phantom, including guidance on what type of catheter to use and how to insert it and secure it in place. Steps to create an acceptable treatment plan for dosimeter irradiation follow. The physicist is instructed to use 10 consecutive dwell positions spaced 5 mm apart, which matches the standard plan used for phantom characterization. No dwell times are listed; it is suggested that the physicist performing the irradiation sets the treatment planning system to optimize dwell times in order to deliver 100 cGy to a line 2 cm away from the catheter channel. An example treatment plan isodose distribution is shown to provide guidance.

2.6.2. Irradiation Form

The Irradiation Form provides space for the physicist performing the irradiation to provide details about his or her system, source, and treatment plan. It is shown in Appendix 6.3.2 and is intended to closely resemble existing forms supplied by the RPC for similar remote audit programs.

The first section asks for simple demographic information about the physics contact, so that the RPC may contact him or her later with any additional questions. The next section includes spaces for the physicist to fill in information about the particular afterloader model, source, and planning system in use. It is also in this section that the physicist shall record the air-kerma strength of the source at the time of dosimeter irradiation. A final section of the irradiation form includes spaces for the physicist to record the planning system-generated dwell times and the reported point dose at the point of measurement.

2.6.3. Questionnaire

Since the proposed outcome of this project is a tool suitable for use as a new RPC outreach program, the remote audits performed in this work also included a survey and questionnaire for the participating physicists to record their opinions of the program prototype. The questionnaire is included in Appendix 6.3.3. Physicists were asked to record their agreement with certain statements on a scale of 1 to 5, with 1 indicating that they strongly disagreed with the statement and 5 indicating that they strongly agreed with the statement. The statements covered a variety of considerations, including clarity of instructions and forms, ease-of-use of the phantom, and understanding of the goals and relevancy of the program. Participating physicists were also asked to record the approximate amount of time that they spent performing the audit, and to include comments or suggestions on setup, planning, and general issues.

3. Results

3.1. Phantom Prototype

The final prototype was designed and manufactured as an 8 × 8 × 10 cm^3 rectangular prism made of High Impact Polystyrene (HIPS) (Boedeker Plastics, Shiner, TX). It is shown in Figure 3.1. HIPS was chosen because it is very durable, relatively inexpensive compared to more specialized materials such as Solid Water, and easily machinable. The RPC has experience with polystyrene phantoms and phantom inserts in a number of previous projects[55, 56]. Crucially, the dosimetric properties of HIPS in the ^{192}Ir energy range closely approximate those of water. Its physical density is 1.04 g/cm^3, just 4% more dense than water. ICRU Report 44[57] defines as water-equivalent any material which introduces uncertainties of ≤1% to absorbed dose. Meli *et al.*[53] found the photon energy spectrum in polystyrene from an ^{192}Ir source to be "essentially identical" to that found in water and declared polystyrene to be a suitable phantom material for ^{192}Ir dosimetry even in the absence of full scatter conditions. Tedgren and Carlsson[46] observed water-equivalence throughout a cylindrical polystyrene phantom of height 20 cm and diameter 20 cm and commented that "the difference between water and plastic is more pronounced for large phantoms".

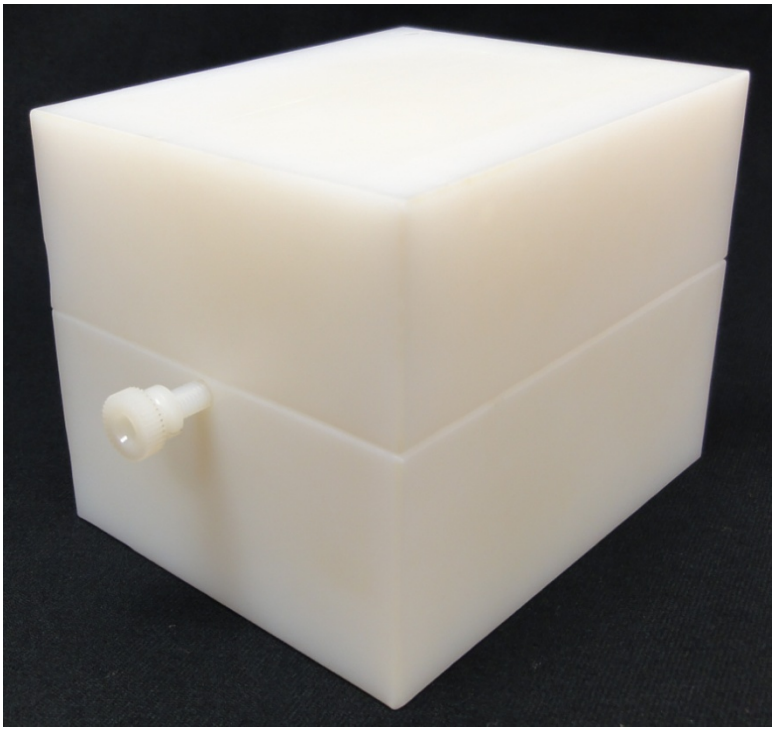

Figure 3.1: The phantom prototype. The thumbscrew through which a 6 French endobronchial catheter may be inserted is at left.

The interior of the phantom has two key features. The first is a cylindrical channel, approximately 85 mm long and slightly greater than 2 mm in diameter. The channel length and the overall phantom length were chosen so that approximately 25 mm of phantom material extends beyond a 45 mm-long tandem source train in both the distal and proximal directions. The channel is drilled into the phantom parallel to its longest dimension and with the opening centered on one of the 8 × 8 cm^2 faces. The diameter is just large enough to admit a standard 6 French (2 mm diameter) endobronchial catheter. A thumbscrew is tapped into the opening of the channel; a catheter may be inserted longitudinally through the thumbscrew and secured from being pulled out of the channel by gently tightening the thumbscrew.

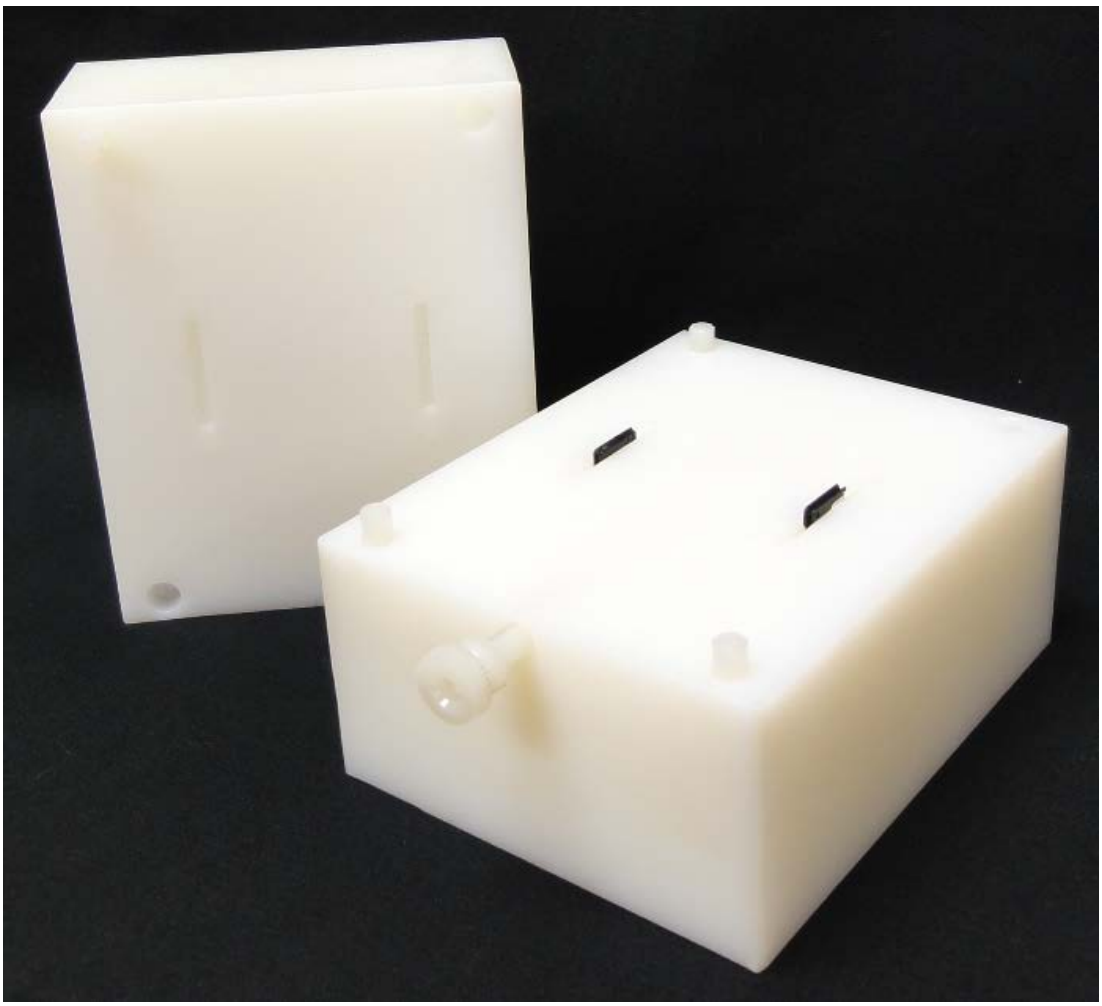

Figure 3.2: The phantom after being pulled apart into its two sections. One nanoDot dosimeter has been inserted into each slot.

The second internal feature of the phantom is a pair of slots carved out of the material, positioned symmetrically on either side of the central channel. Using two dosimeters for each

measurement – one in each slot – greatly reduces the uncertainty introduced due to the source moving from side-to-side (laterally) inside the channel. Each slot is slightly larger than 10 × 10 × 2 mm^3, just large enough to admit a single nanoDot OSL dosimeter of the type used in this experiment. The slots are oriented with one of their long axes parallel to the central channel and their short axes perpendicular to it, such that they "face" the channel. Each is situated with its midpoint exactly 20 mm toward the edge of the phantom away from the midpoint of the diameter of the channel. This distance was chosen because it is on the order of typical clinically-relevant distances (e.g. Point A in the Manchester system[58]) and for planning purposes which will be discussed below. An additional 20 mm of polystyrene extends beyond the slots opposite the source to provide material for photon backscatter. The slots are centered within the phantom in the other two dimensions. As shown in Figure 3.2, the phantom separates lengthwise into two unequally-sized pieces of height 44 mm and 36 mm, exposing approximately 1 mm of the top of an inserted dosimeter for ease in loading and removal. Note that the catheter channel is entirely buried in the 44 mm-tall section and only its entrance is exposed to air. A cross-sectional top view of the phantom is shown in Figure 3.3 and additional views are presented in Appendix 6.1.

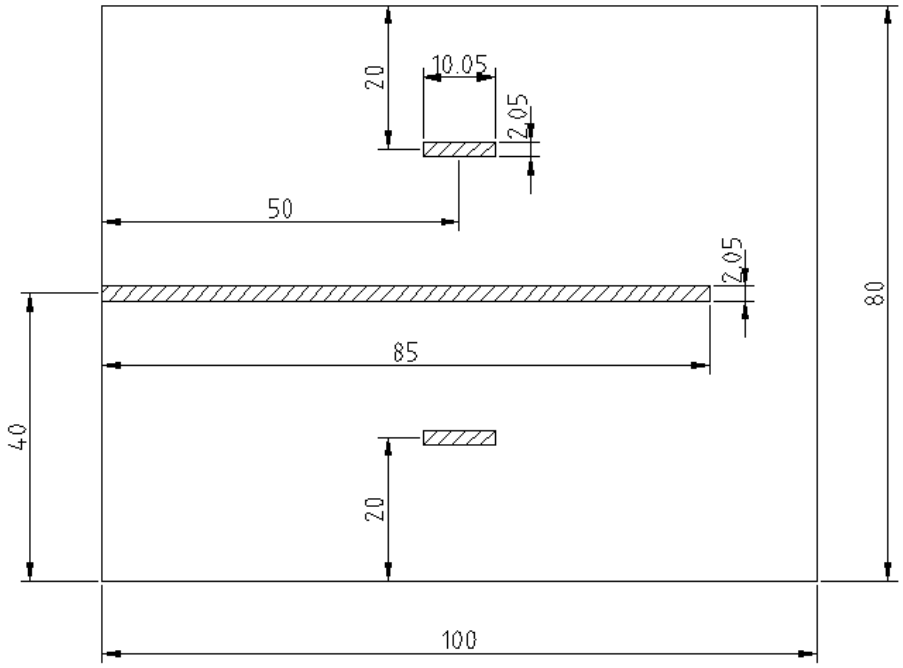

Figure 3.3: A cross-sectional top view of the phantom, showing its dimensions. All measurements are in mm. Shaded areas are the carved-out areas forming the central channel and two OSLD slots. Additional views may be found in Appendix 6.1.

3.2. Linearity Correction Factor K_L

The total number of dosimeters irradiated across all three trials performed in the determination of K_L was 78, and the breakdown by trial number and delivered dose is shown in Table 2.1. An example of the un-normalized dose response data for Trial 2 with its corresponding linear fit is shown in Figure 3.4.

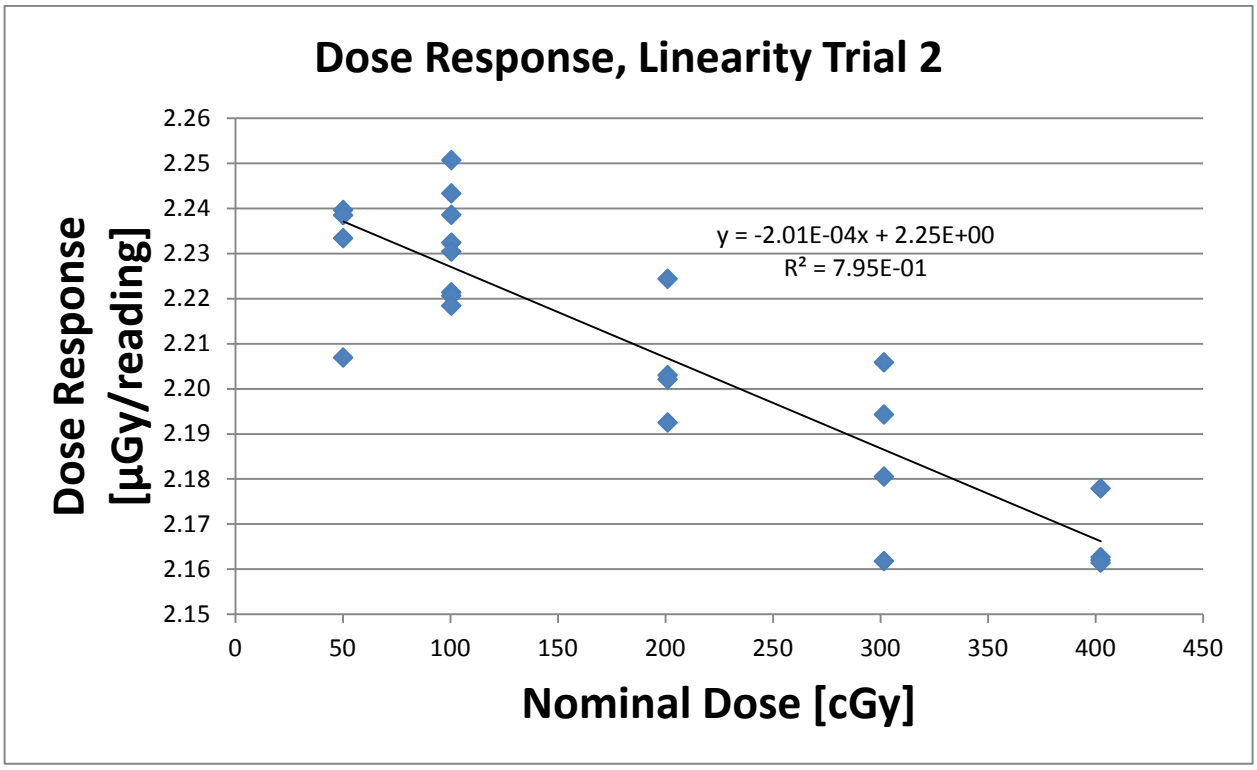

Figure 3.4: OSLD dose response versus nominal dose, 2nd trial of 3.

The linear fit of the dose response for each of the three Trials is shown in Equations 3.1-3.3.

$$Dose\ Response\ (1) = (-2.103 \times 10^{-4}) \times Nominal\ Dose + 2.224 \qquad R^2 = 0.62 \qquad (3.1)$$

$$Dose\ Response\ (2) = (-2.013 \times 10^{-4}) \times Nominal\ Dose + 2.247 \qquad R^2 = 0.79 \qquad (3.2)$$

$$Dose\ Response\ (3) = (-2.268 \times 10^{-4}) \times Nominal\ Dose + 2.240 \qquad R^2 = 0.55 \qquad (3.3)$$

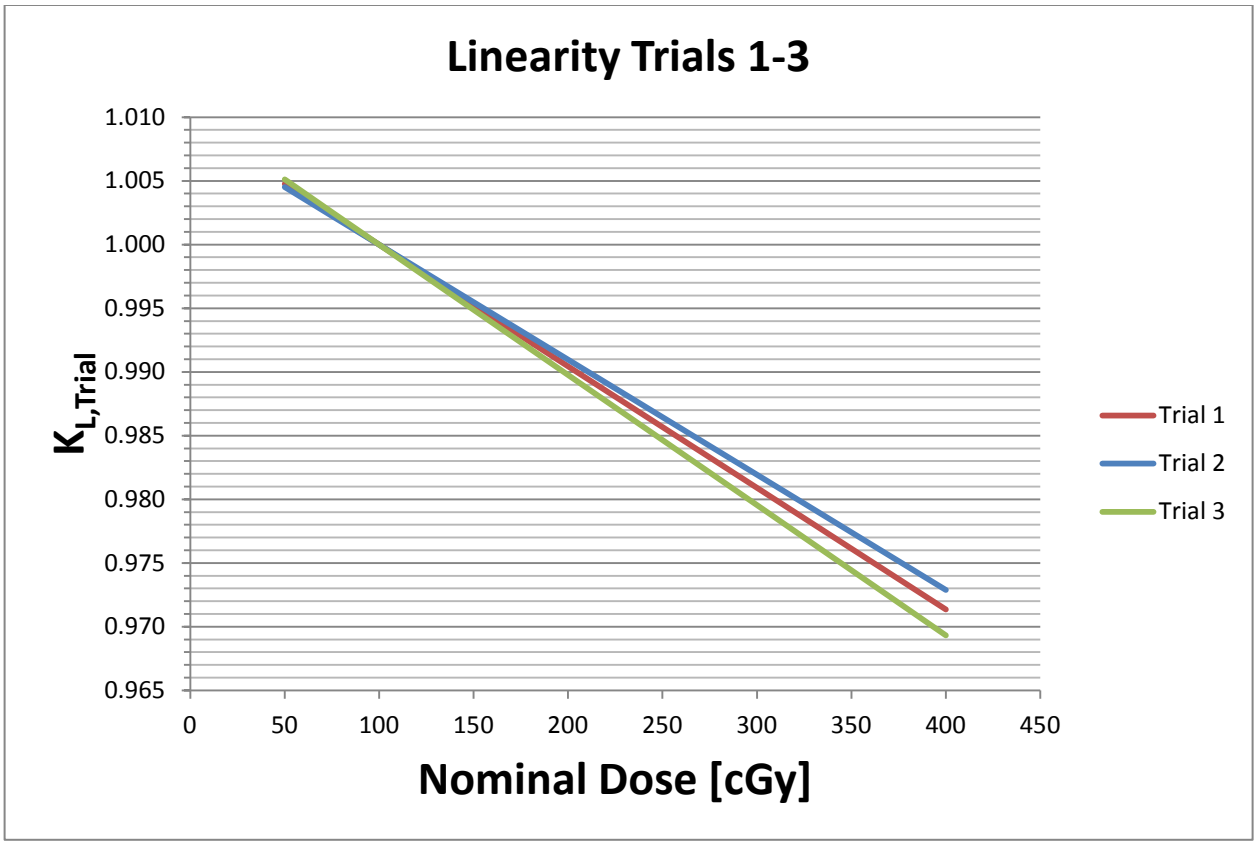

Figure 3.5: Linearity correction factors determined separately for each of three trials.

The $K_{L,Trial}$ lines determined for each trial after normalization are shown in Figure 3.5. Each trial was individually normalized such that at a nominal dose of 100 cGy, K_L = 1.000. The agreement among the three trials was very good. For Trials 2 and 3, the values of $K_{L,Trial}$ at 50 cGy were less than 0.06% different, and the values at 400 cGy were less than 0.37% different. The line calculated from Trial 1 fell between those of Trial 2 and Trial 3.

After verifying their agreement with one another, the three linearity trials were combined into a single data set. A linear fit of the form $dose\ response = (\alpha \times d) + \beta$ where *d* is the nominal dose was applied to the combined non-normalized data. The values of the fit parameters were $\alpha = -2.090 \times 10^{-4}$ and $\beta = 2.236$ with R^2 = 0.58. The combined data dose response plot is shown in Figure 3.6.

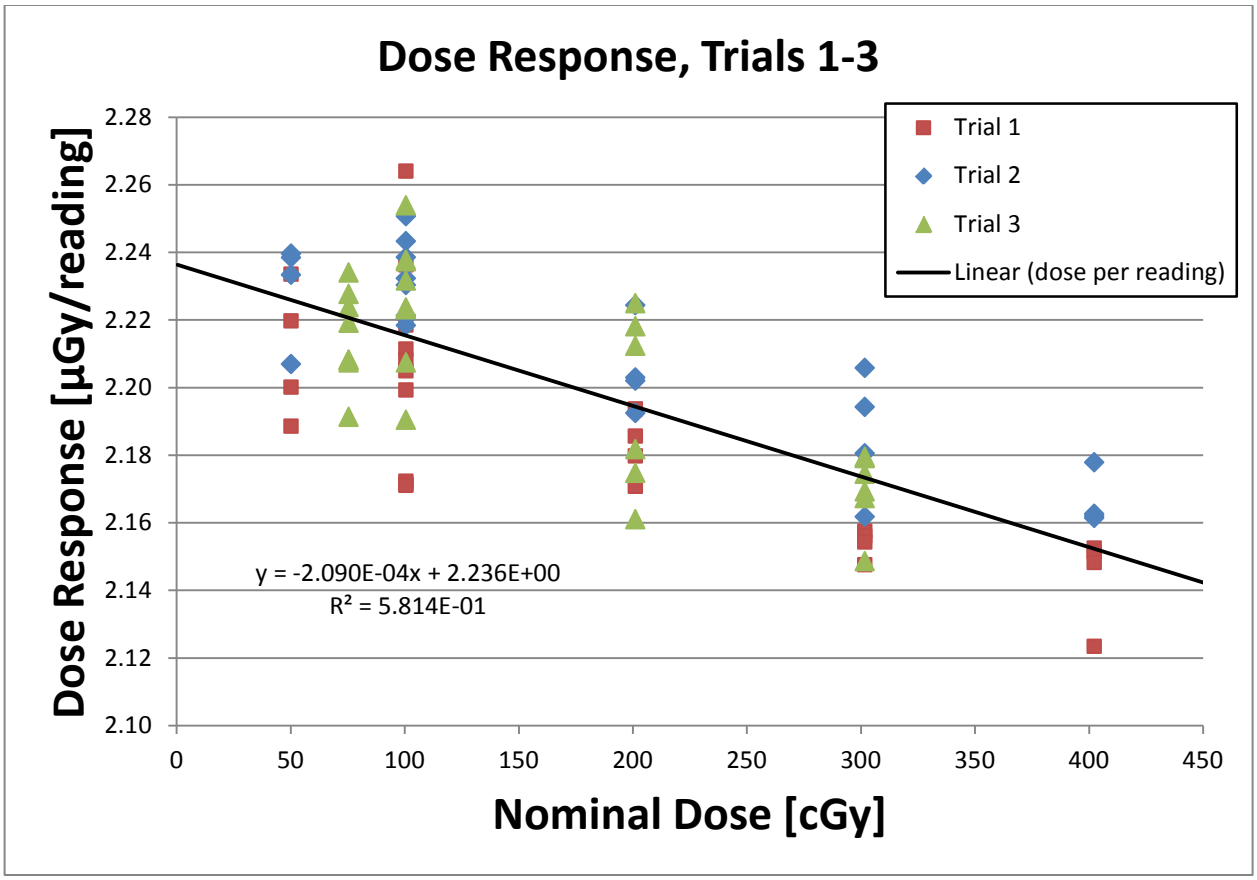

Figure 3.6: The dose response for linearity trials 1 through 3. Data points for each trial are shown in different colors but considered as a single combined data set for the purposes of linear fitting.

This fit was then normalized to 1.000 at 100 cGy and the resulting normalized linear fit is the final linearity correction factor, K_L. This plot is shown in Figure 3.7 and Figure 3.8 along with the 68% and 95% confidence intervals of the fit. Assuming that OSLD readings follow a normal distribution, these confidence intervals represent one and two standard deviations, respectively. The final fit equation for K_L is given in Equation 3.4:

$$K_L = (-9.433 \times 10^{-5} \times dose) + 1.009 \tag{3.4}$$

where *dose* is the nominal dose in cGy.

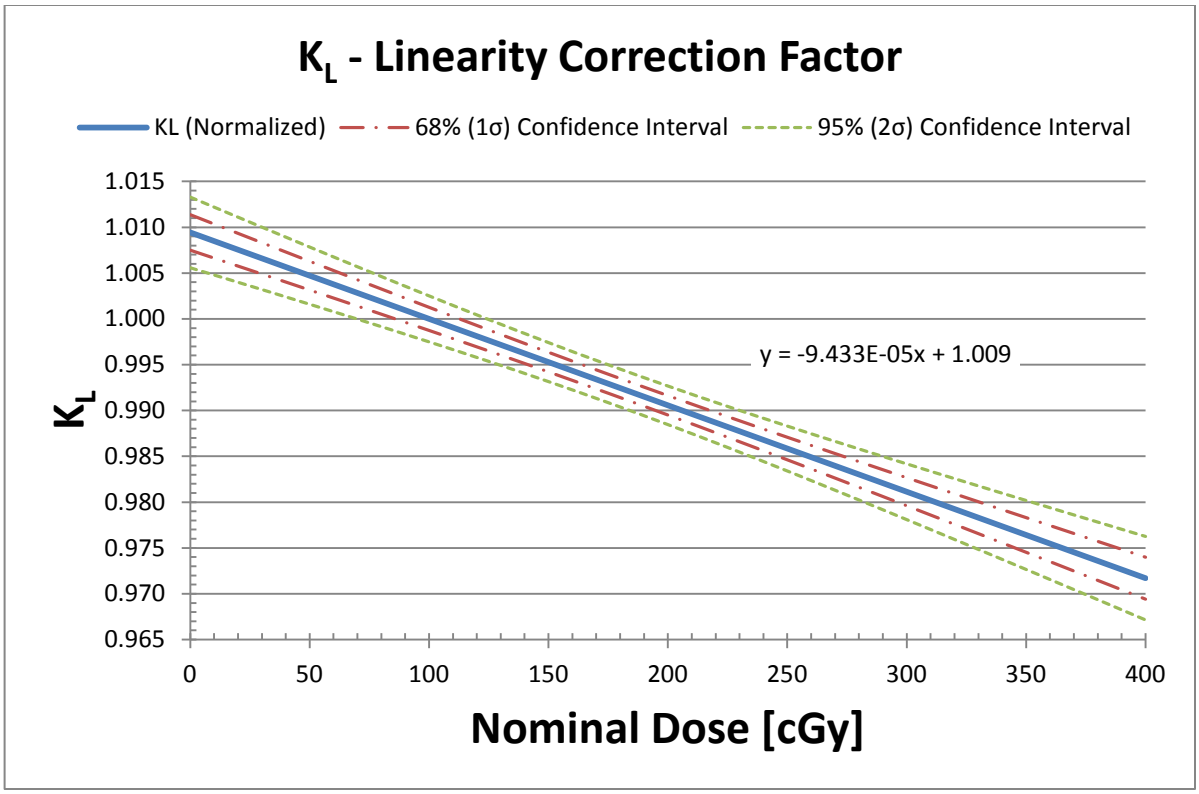

Figure 3.7: Final linearity correction factor K_L based on three independent trials. The dashed lines represent the 68% (1σ) and 95% (2σ) confidence intervals for the linear fit.

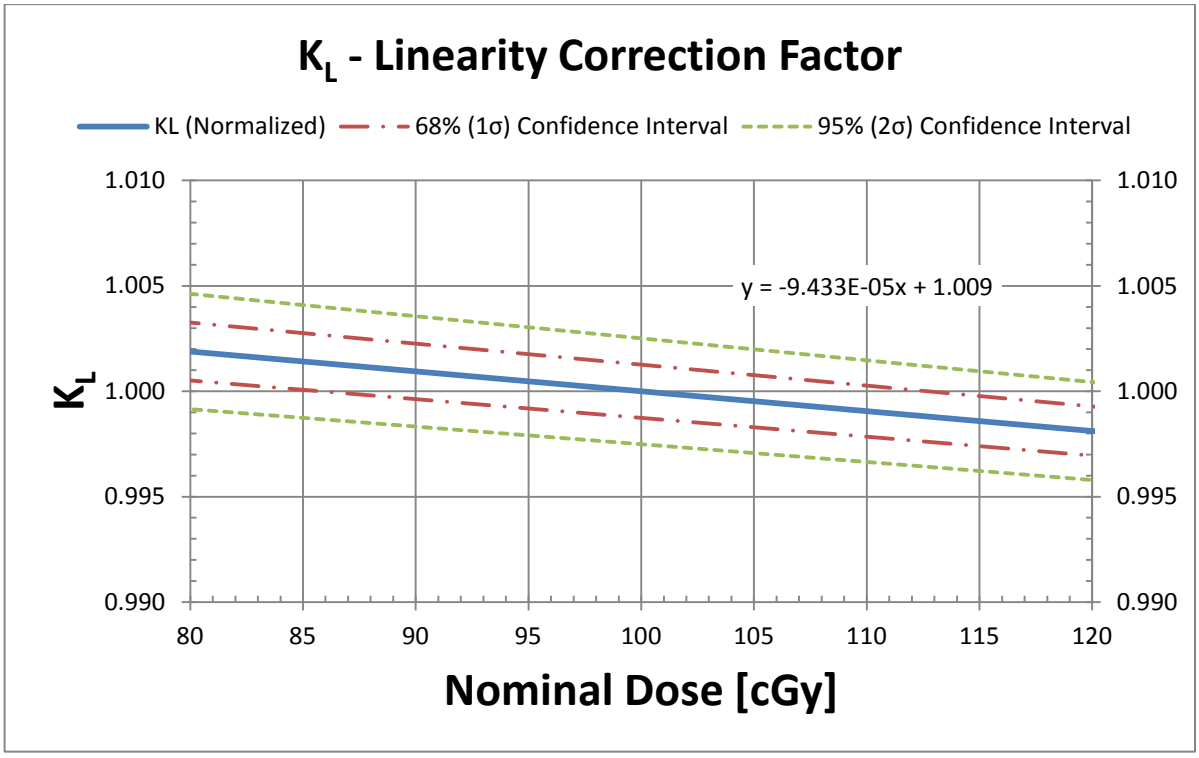

Figure 3.8: Final linearity correction factor K_L based on three independent trials. This is the same plot as Figure 3.7 but showing only the region between 80 and 120 cGy nominal dose.

The 68% confidence interval of the linear fit for K_L spans approximately 0.3%, or ±0.15% in the region from 90 to 110 cGy, as shown in Figure 3.8. Because the proposed audit program will require institutions to attempt to deliver a dose of 100 cGy at the point of measurement, we may assume that σ = ±0.15% is the expected uncertainty in the linearity correction factor (68% CI, representing a single standard deviation assuming the data follow a normal distribution). This is the value that will be used in the final system uncertainty calculation which may be found below.

3.3. Block Correction Factor K_B

The results of 20 measurements to obtain the Nucletron-specific block correction factor $K_B^{Nucletron}$ are shown in Table 3.1.

Table 3.1: K_B statistics for a Nucletron source.

$K_B^{Nucletron}$	
n	20
Average	1.026
Minimum	1.017
Maximum	1.036
Standard Deviation	0.006 (0.6%)
Standard Error	0.001 (0.1%)
99% Confidence Interval	1.022 – 1.029

Likewise, the results of 10 measurements of K_B^{Varian} are shown in Table 3.2.

Table 3.2: K_B statistics for a Varian source.

K_B^{Varian}	
n	10
Average	1.000
Minimum	0.992
Maximum	1.013
Standard Deviation	0.007 (0.7%)
Standard Error	0.002 (0.2%)
99% Confidence Interval	0.993 – 1.007

The difference between $K_B^{Nucletron} = 1.026$ and $K_B^{Varian} = 1.000$ is approximately 2.6%; the reasons for this difference are discussed below. For all dose measurements performed in this work and the trial audits, the appropriate K_B was selected based on the source model used to irradiate the dosimeters. A histogram of all K_B measurements for both the Nucletron and Varian source is shown in Figure 3.9.

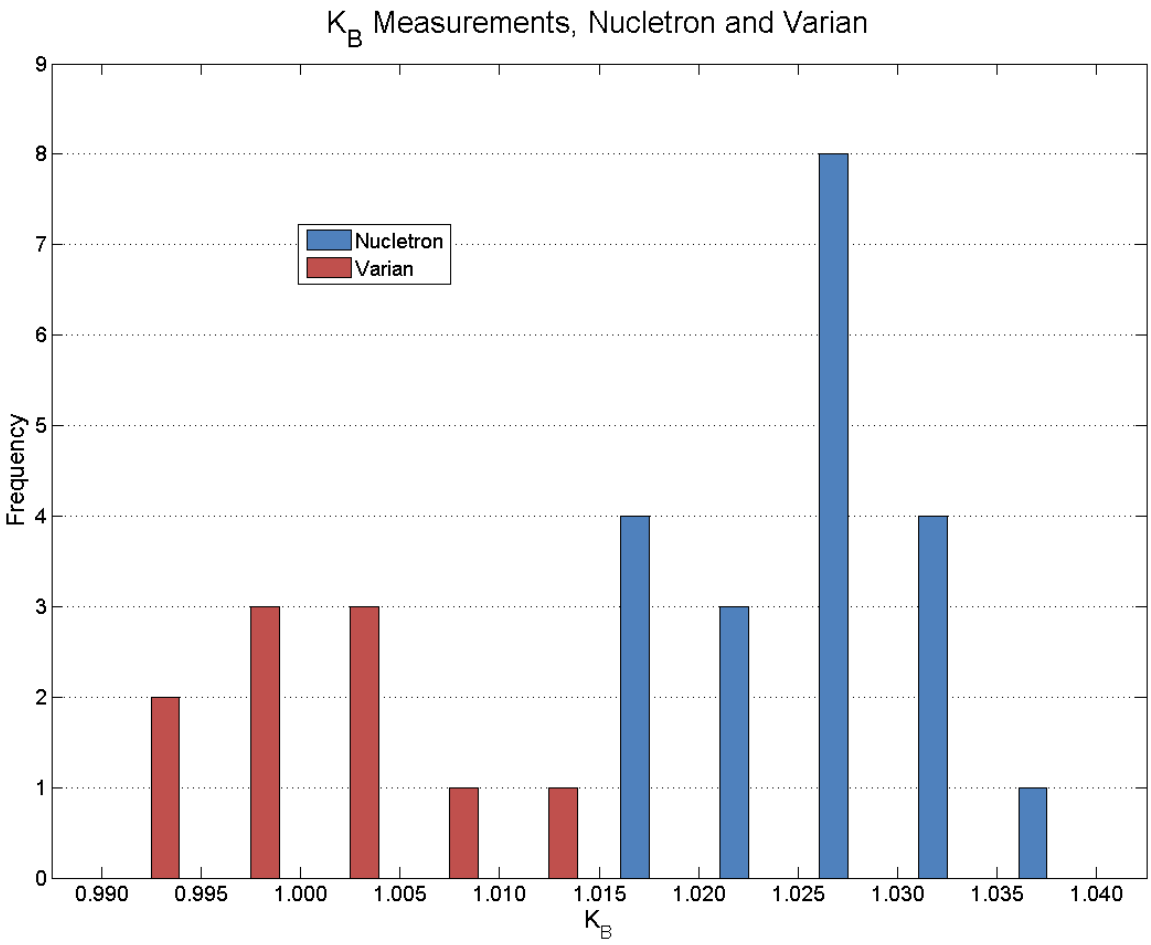

Figure 3.9: Histogram showing both $K_B^{Nucletron}$ (n=20) and K_B^{Varian} (n=10) values.

3.4. Dose Rate Effect

The measured-to-expected dose ratios for a number of independent irradiations collected over the course of the study are shown in Figure 3.10 plotted against the calibrated source strength at the time of irradiation. All irradiations were performed with a Nucletron source.

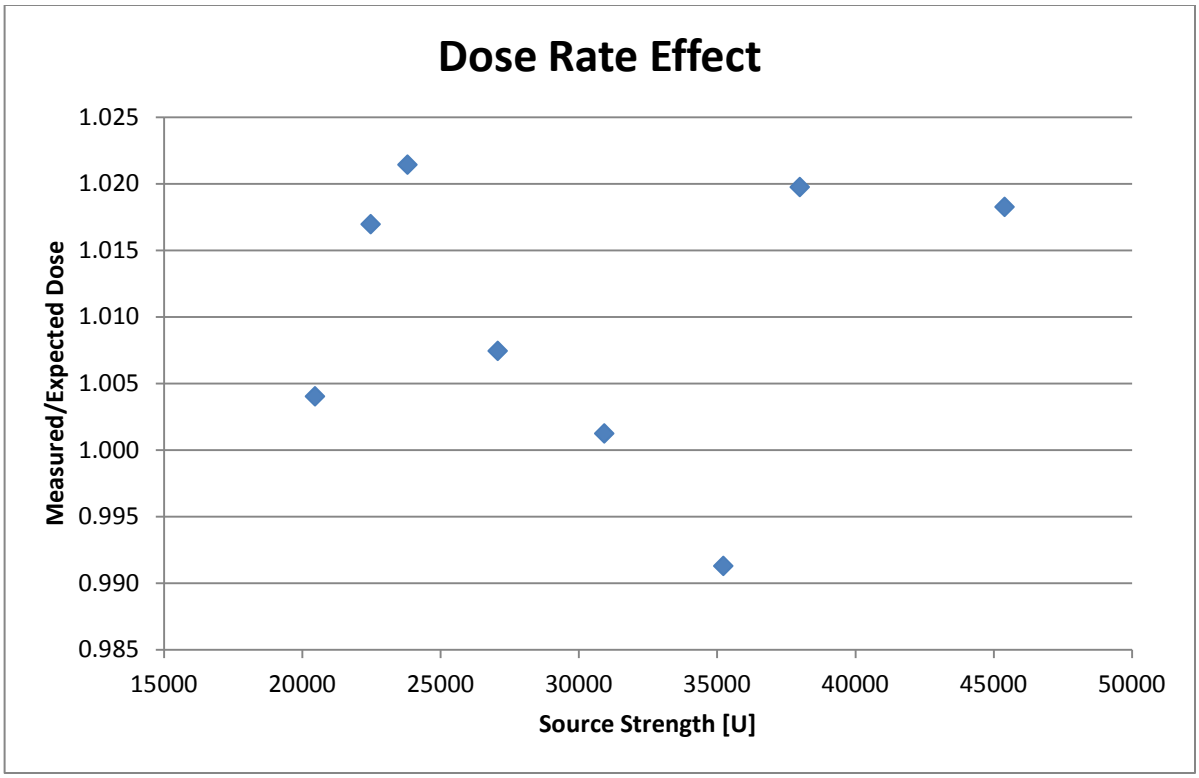

Figure 3.10: The measured-to-expected dose ratio of several measurements plotted versus the source strength at the time of measurement. These data were collected with the same Nucletron source as it decayed over time.

An F-test found that there is no statistically-significant difference between the slope of the linear best fit line for these data and 0 ($p = 0.88$).

3.5. Phantom Characterization

3.5.1. OSLD Orientation

Average doses among the measurements made at each of the 8 possible OSLD orientations ranged from 50.77 cGy to 51.41 cGy. A one-way analysis of variance (ANOVA) showed no statistically significant difference between the means of each individual orientation and the overall mean ($p = 0.998$). This finding is consistent with expectations as the front and back of the nanoDot cassette are made of the same material in the same thickness, and the active dosimeter is assumed to be positioned at the midway point of the cassette width. The active dosimeter is off center in the large face of the cassette, however any deviation due to this positioning should be minimal as the shift is relatively small (approximately 1 mm off center in each dimension) and the isodose distribution in the region of the active dosimeter is rather flat by design.

3.5.2. Source Position

The relative dose measurements made with the source train in various positions along the distal/proximal axis are shown in Figure 3.11.

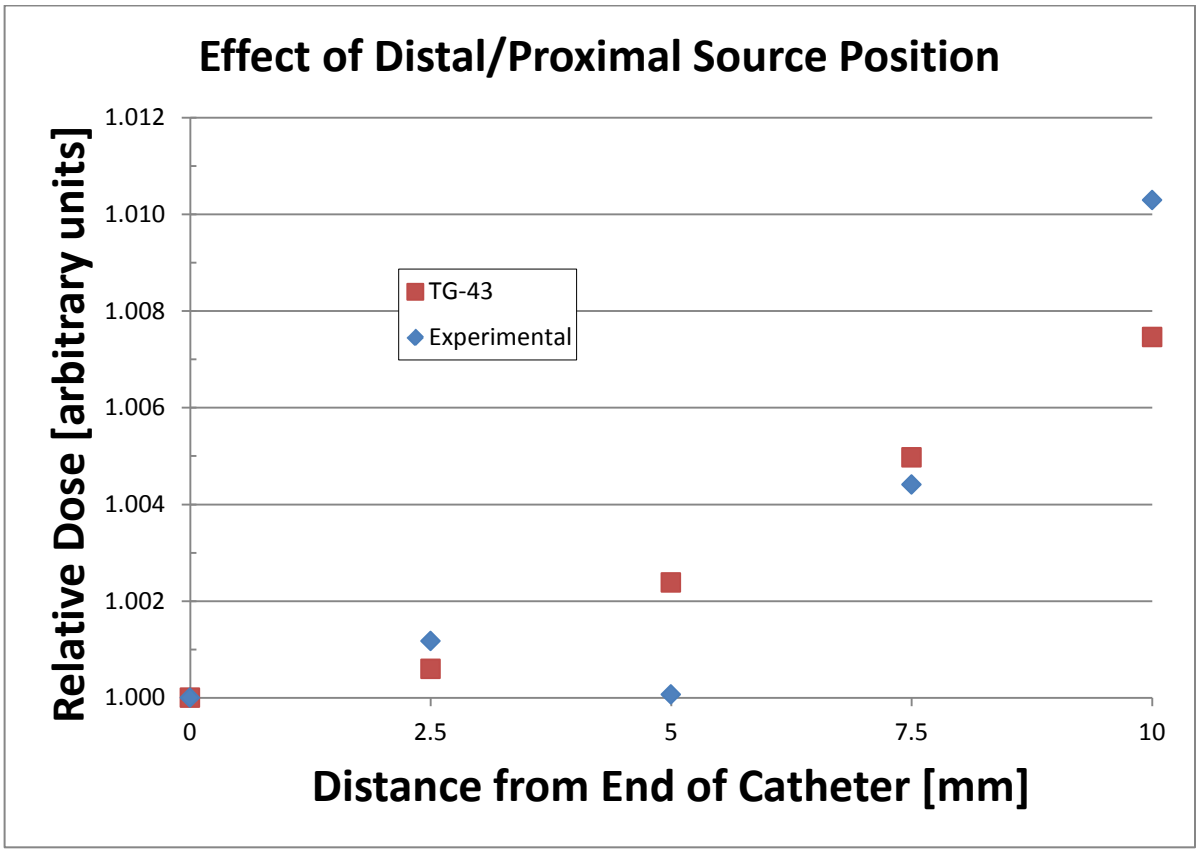

Figure 3.11: The effect of variations in placement of the source train along the distal/proximal axis. Both experimental results and TG-43 calculations are shown.

Ending the source train 5 mm short of the intended farthest distal extent resulted in a negligible change in dose. An error of 10 mm in placing the catheter results in an overdose of approximately 1%, well less than the estimated overall accuracy limits of the system. The minimal effect of a 10 mm shift in the position of the source train is in line with expectations because of the nature of the standard plan used for irradiation. The dwell times of the plan were optimized to deliver 100 cGy to a line 4.5 cm long and 2 cm away from the central channel so the 100 cGy isodose line follows this prescription line closely for almost its entire 4.5 cm extent. Thus even relatively large shifts in the positioning of the source train in the distal/proximal direction still result in some dose close to 100 cGy being delivered to the point of measurement.

3.6. Retrospective Dose Calculations

Using the correction factors K_L, $K_B^{Nucletron}$, and K_B^{Varian}, the measured OSLD dose was retrospectively calculated for several irradiations performed during the course of this study, regardless of purpose. The measured doses were compared to the expected doses, which was the dose calculated using TG-43, the actual dwell times used during irradiation, and the calibrated source strength. The results are given in Table 3.3.

Table 3.3: Results from retrospective dose calculations of 23 measurements made for various purposes over the course of this work.

Data Set	Source	n	Average Measured Dose [cGy]	Dose Standard Deviation	Measured/Expected Dose [cGy]
A	Nucletron	5	104.1	1.404	1.027
B	Nucletron	4	102.5	1.320	1.005
C	Nucletron	4	102.1	0.533	1.004
D	Nucletron	4	102.7	0.910	1.013
E	Nucletron	6	100.3	0.582	0.989
Total		23	102.2	0.938	1.007

3.7. Trial Remote Audits

3.7.1. Dosimetry

Table 3.4: Results of eight trial remote audits at separate institutions. All doses are in cGy.

Trial	Source Model	RPC Measured Dose [cGy]	Institution Reported Dose [cGy]	TG-43 Calculated Dose [cGy]	RPC/Institution
1	Nucletron	99.9	101.0	100.1	0.989
2	Varian	100.4	99.9	100.1	1.005
3	Varian	100.0	99.9	100.1	1.001
4	Nucletron	100.5	100.6	100.8	0.999
5	Nucletron	102.1	100.7	100.9	1.014
6	Varian	98.3	100.0	98.6	0.983
7	Nucletron	101.3	100.1	99.7	1.012
8	Varian	99.4	99.8	99.5	0.996
				Average	**1.000**
				Standard Deviation	**0.011**

The results of eight remote audits are shown in Table 3.4. The RPC Measured Dose is that measured with OSLDs. The Institution Reported Dose is that reported by the institution's treatment planning system at the point of measurement. Finally, the TG-43 Calculated Dose is that calculated independently using the source strength and dwell times that the institution reported to the RPC.

The RPC Measured Dose to Institution Reported Dose ratios range from 0.983 to 1.014 for the eight institutions audited. Average of all eight ratios was 1.000 with a standard deviation of 0.011.

3.7.2. Questionnaires

On a scale of 1 to 5, with 1 indicating “strongly disagree” and 5 indicating “strongly agree”, the average response to the 11 statements on the feedback questionnaire ranged from a minimum of 3.9 to a maximum of 4.8. Median scores for the 11 statements ranged from 4 to 5. The average agreement across all respondents and all statements was 4.3 and the standard deviation was 0.7. Not all respondents responded to all statements. In general, higher scores indicated positive feelings toward the project, including favorable opinions of instruction clarity and ease-of-use, and interest in the tool as a potential RPC audit program. All responses to the questionnaire are collected in Appendix 6.4.

Respondents were also asked to give an estimate of the total time they spent in performing the audit, including planning, setup, irradiation, and completing forms. The reported times ranged from 15 to 120 minutes, with an average of 69 minutes. The median was 60 minutes. Lastly, respondents were asked to optionally provide comments, suggestions, and concerns regarding the project. These free-form responses are included in full in Appendix 6.4 as well.

4. Discussion

4.1. Linearity Correction Factor

The linearity correction factor determined here differs from that determined by the RPC for the same batch of dosimeters and used in the external beam remote audit program, reprinted here from Equation 2.8.

$$K_L^{RPC} = (-1.374 \times 10^{-4} \times dose) + 1.013 \tag{2.8}$$

The linearity correction factor and the RPC's correction factor for the same batch of dosimeters are shown in Figure 4.1 along with the underlying data.

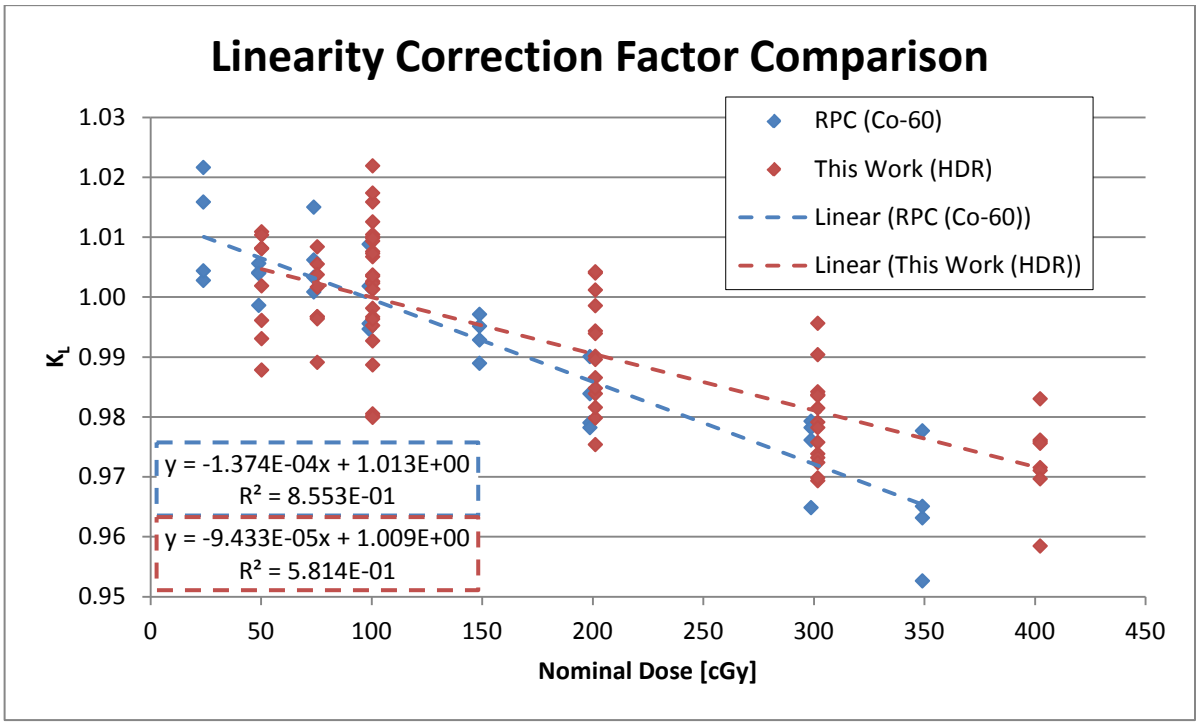

Figure 4.1: A comparison of the linearity correction factor determined in this work and that determined by the RPC for the same batch of dosimeters.

The RPC has previously documented variations in linearity within a single batch of dosimeters after irradiation under different spectra[59]. The possibility that some relationship exists between linearity and irradiation energy contradicts certain RPC assumptions and further investigation is needed in this area. However, the important implication here is that for each new batch of dosimeters commissioned for use with the HDR phantom created in this project, a new linearity correction factor must be determined using the methods outlined in Section 2.4.4. It

cannot be assumed that K_L for HDR sources will necessarily match the RPC's ^{60}Co-based linearity correction factor for the same batch of dosimeters.

In the process of commissioning the phantom described here as a new RPC audit program, linearity measurements were made using a different batch of dosimeters from the batch used throughout this work. Again, the HDR linearity correction factor differed from that determined for the same batch of dosimeters using a ^{60}Co beam. Cobalt-60 and HDR linearity correction factors are shown for both the batch used in this work and the new batch in Figure 4.2.

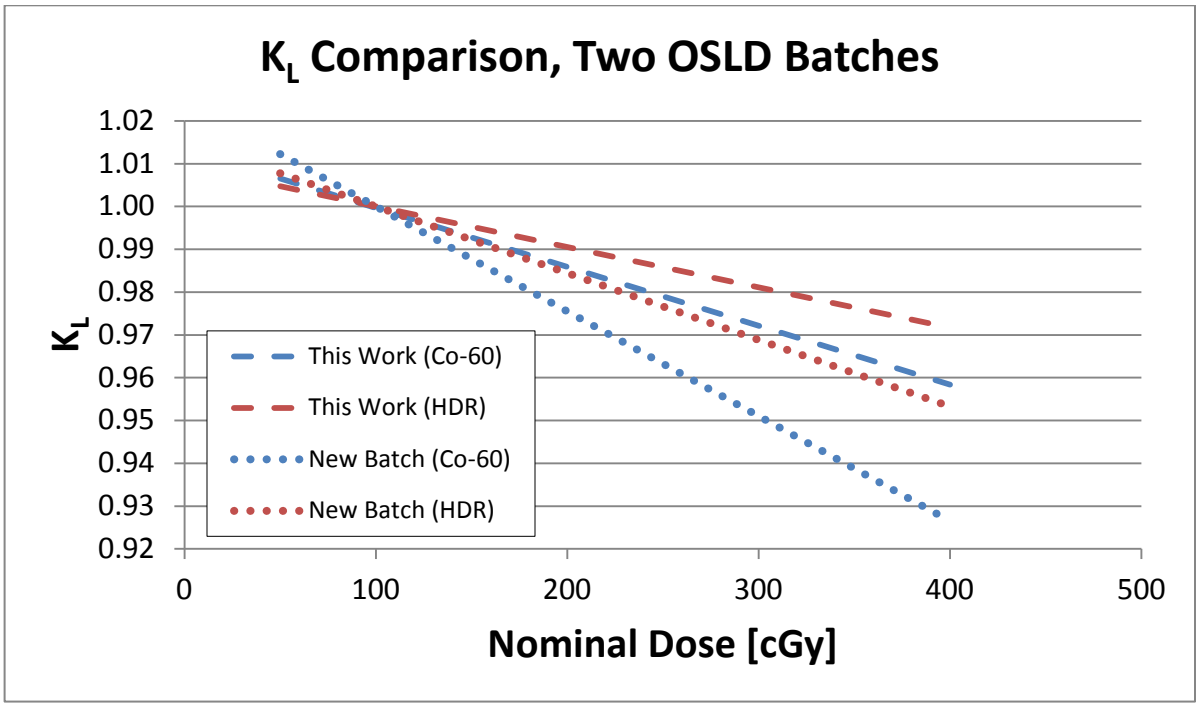

Figure 4.2: Comparison of linearity correction factors determined for two different OSLD batches. Dashed lines represent the batch used throughout this work. Dotted lines represent a new batch currently being commissioned at the RPC. Blue lines represent correction factors determined using a ^{60}Co beam and a specially-designed acrylic block. Red lines represent correction factors determined using an ^{192}Ir HDR source and the phantom described in this work.

In the case of both batches, the slope of the HDR linearity correction factor was less than that of the ^{60}Co K_L. It is important to note that for each new batch of dosimeters to be used with the HDR phantom created in this project, a new linearity correction factor will need to be determined as K_L cannot be expected to match the RPC's linearity correction factor for the same batch.

4.2. Block Correction Factor

Jursinic[10] found OSLDs to be 6% more sensitive under ^{192}Ir irradiation when compared to 6 MV x-rays. This disagrees with the block correction factors determined in this work, which were 1.026 and 1.000 for Nucletron and Varian sources, respectively. Energy correction is assumed to be a major component of those two block correction factors. However, in contrast to the energy correction of Jursinic, the factors determined here also account for several other corrections, as detailed in Section 2.4.5. Among these are the differences between dosimetry in polystyrene and in water, the angular dependence of OSLD nanoDots, and a phantom size that is too small to provide full scatter conditions. All of these considerations are irrelevant to the work of Jursinic.

A key finding is the need for vendor-specific block correction factors to improve the accuracy of dose measurements. This result likely arises from differences in source geometry and encapsulation. The Nucletron source consists of cylindrical core of iridium of length 3.60 mm and diameter 0.65 mm[47]. The density of iridium is 22.56 g/cm^3. The radioactive ^{192}Ir is distributed uniformly in the core, which is encapsulated by a 0.125 mm-thick sheath of AISI 316L stainless steel (68% Fe, 17% Cr, 12% Ni, 2% Mn, 1% Si by weight). The density of the steel encapsulation is 8.02 g/cm^3.

The Varian source consists of two cylindrical iridium sources with hemispherical ends situated in tandem[49]. Each source is 2.50 mm long and 0.34 mm in diameter. The radioactive ^{192}Ir is uniformly distributed in the cores. The sources are encapsulated at the end of a Ni/Ti wire (55.6% Ni, 44.4% Ti by weight) with a diameter of 0.59 mm. Thus the thickness of the encapsulation is 0.125 mm around the sources. The density of the wire is 6.5 g/cm^3.

As the density thickness of both the source itself and the encapsulation material is greater for the Nucletron source, we may expect that it attenuates the ^{192}Ir spectrum slightly more than the Varian source. Indeed, Rivard *et al.*[60] found the water-kerma of the Varian source to be 5.0±0.2% higher than that of the Nucletron source for equivalent spectra and attributed this difference to the thickness of the iridium cores. Rasmussen *et al.*[61] noted that the Varian source emits a spectrum with a slightly higher average energy than the Nucletron source, likely due to less self attenuation in the source, and also remarked on its reduced polar anisotropy compared to the Nucletron source. Thus it is not unexpected that $K_B^{Nucletron} \neq K_B^{Varian}$. It is important to note that should any new source models be introduced into clinical use, it is likely that a new block correction factor will

need to be determined for the new source, especially if its physical dimensions and encapsulation differ substantially from those of the current Nucletron or Varian sources.

Block correction factors were also determined for a new OSLD batch currently being commissioned for use with the HDR phantom at the RPC. The $K_B^{Nucletron}$ for the new batch was found to be 1.035, or about 0.9% higher than the value found for the OSLD batch used in this work. Likewise, K_B^{Varian} for the new batch was 1.004 or 0.4% higher than the value found in this work. The difference between the block correction factors for the two sources was 3.1% for the new batch, compared to 2.6% for the batch investigated in this work. In the future, it should not be assumed that block correction factors are independent of OSLD batch, and for each new OSLD batch commissioned by the RPC, new block correction factors for each source must be determined.

4.3. Dose Rate Effect

This work found that OSLD-measured dose had no dependence on dose rate as represented by source strength, which has a direct relationship to dose rate for brachytherapy sources. This is in agreement with sources in the literature that also found no such dependence[10, 62, 63]. Thus no correction factor for dose rate needs to be included in Equation 2.6 to accurately calculate dose. The tool described here and the formalism of Equation 2.6 is sufficient to remotely audit HDR sources at any clinically-relevant source strength.

4.4. Trial Audits

4.4.1. Dosimetry

The dosimetry results from trial remote audits indicate that the phantom created in this work, when used with nanoDot OSLDs, can accurately measure dose when used in a mailable audit program. The average difference between dose measured using the tool and the institutionally-reported treatment planning system for the eight institutions audited was negligible (RPC-to-institution ratio = 1.000). Assuming that dose measurements are normally-distributed, more than 95% of all measurements will fall within two standard deviations of the mean, which for the eight trial audits performed in this work was approximately ±2.2%.

For 193 well-chamber measurements of HDR source strength performed by the RPC from 1994 to 2011, the average RPC-to-institution ratio was 1.009. The standard deviation was 0.014,

thus the 2σ percent uncertainty was approximately 2.8%. The results from the audits performed using the phantom developed in this work are on average closer to the institution's reported value (1.000 versus 1.009) and with a smaller standard deviation (0.011 versus 0.014) than the RPC's well-chamber measurements.

4.4.2. Questionnaire Feedback

The results from the trial audit questionnaires reveal that in general, physicists had a good understanding of how to plan and use the phantom and what tasks they needed to complete for a successful audit. Respondents' average level of agreement with the statements on the questionnaire were in general between "somewhat agree" and "strongly agree", with only the occasional rating lower than those levels. This indicates that the design of the phantom was intuitive enough and the included instructions clear enough to direct physicists to properly irradiate the phantom the majority of the time.

4.5. Uncertainty Analysis

Equation 2.6, by which dose is calculated from an OSLD reading is repeated here:

$$Dose = (avg.corrected\ rdg.) \times ECF \times Sensitivity \times K_F \times K_L \times K_B \tag{2.6}$$

where the system *Sensitivity* is a compound term with an equation of its own (Equation 2.7):

$$Sensitivity = \frac{Expected\ Dose\ to\ Standard}{avg(avg.corrected\ reading) \times K_F \times K_L^{std}} \tag{2.7}$$

Aguirre *et al.*[7] have already determined the individual percent uncertainties for each term in Equation 2.7. Adding these uncertainties in quadrature gives the expected percent uncertainty in the system sensitivity, $\sigma_{Sensitivity}$:

$$\begin{aligned} \sigma_{Sensitivity} &= \sqrt{\sigma_{dose\ to\ std}^2 + \sigma_{avg\ rdg}^2 + \sigma_{K_F}^2 + \sigma_{K_L^{std}}^2} \\ &= \sqrt{0.6^2 + 0.4^2 + 0.3^2 + 0.1^2} \\ &< 0.8\% \end{aligned} \tag{4.1}$$

In Equation 4.1, $\sigma_{dose\ to\ std}$ is the percent uncertainty in the dose delivered to a standard dosimeter, $\sigma_{avg\ rdg}$ is the percent uncertainty in the average reading of a pair of standard

dosimeters, and σ_{K_F} and $\sigma_{K_L^{std}}$ are the percent uncertainty in the fading correction factor and the linearity correction factor for standards and controls in the region of 90 to 110 cGy, respectively. The first three terms are all quoted at the level of one standard deviation, and $\sigma_{K_L^{std}}$ is based on the 95% confidence interval of the linear fit for K_L^{std}.

Similarly, adding the uncertainties of each term in Equation 2.6 in quadrature gives the uncertainty in a dose measurement based on an OSLD reading:

$$\sigma_{Dose} = \sqrt{\sigma_{avg\ rdg,inst}^2 + \sigma_{ECF}^2 + \sigma_{Sensitivity}^2 + \sigma_{K_F}^2 + \sigma_{K_L}^2 + \sigma_{K_B}^2} \tag{4.2}$$

Here, $\sigma_{avg\ rdg,inst}$ refers to the percent uncertainty in an average reading of an *institutional* dosimeter, defined as any dosimeter which is not a standard or control. The percent uncertainty of an institutional dosimeter is different from and larger than the percent uncertainty in an average reading of a standard or control dosimeter mentioned above because the irradiation conditions are not as carefully defined. Aguirre provides this figure as well but combines it with the percent uncertainty in the ECF, σ_{ECF}, in a single term. Thus we may say that $\sigma_{ECF} = 0$ and use Aguirre's $\sigma_{avg\ rdg,inst} = 0.57\%$ as the combined uncertainty in the reading and the ECF.

The percent uncertainty in the fading correction factor is the same as that provided by Aguirre. However, the percent uncertainty in the linearity correction factor (σ_{K_L}) depends on the linearity determined specifically in this work and thus differs from Aguirre's uncertainty. In the region of 90 to 110 cGy, the 68% confidence interval in K_L, which represents one standard deviation assuming the data follow a normal distribution, is ±0.15% (see Figure 3.8) so that is the value for σ_{K_L} used here.

Lastly we assume σ_{K_B}, the percent uncertainty in the block correction factor, to equal one standard deviation of the measured K_B in percent. These numbers are 0.6% and 0.7% for the Nucletron- and Varian-specific block correction factors respectively (see Table 3.1 and Table 3.2). The individual uncertainty values may be applied to Equation 4.2 to calculate the overall uncertainty of the system:

$$\begin{aligned}\sigma_{Dose,Nucletron} &= \sqrt{(0.57\%)^2 + (0)^2 + (0.8\%)^2 + (0.3\%)^2 + (0.15\%)^2 + (0.6\%)^2} \\ &= 1.2\%\end{aligned} \tag{4.3}$$

$$\sigma_{Dose,Varian} = \sqrt{(0.57)\%^2 + (0)^2 + (0.8\%)^2 + (0.3\%)^2 + (0.15\%)^2 + (0.7\%)^2} = 1.2\% \quad (4.4)$$

Assuming that OSLD dose measurements follow a normal distribution, 95.45% of all readings will fall within two standard deviations of the mean. Thus we quote 2σ as the estimated uncertainty in the system. This is 2.4% for measurements of Nucletron sources and 2.5% for measurements of Varian sources. The complete uncertainty budget is presented in Table 4.1.

Table 4.1: Uncertainty budget in dose calculations based on OSLD readings as calculated using Equation 2.6. All values given are in percentages.

Quantity	Value (Percent)		Source
$\sigma_{avg\ rdg,inst}$	0.57		Aguirre
σ_{ECF}	0		Aguirre (included in $\sigma_{avg\ rdg,inst}$)
$\sigma_{Sensitivity}$	0.8		Aguirre (see Equation 4.1)
σ_{K_F}	0.3		Aguirre
σ_{K_L}	0.15		68% Confidence Interval of K_L from 90 to 110 cGy (see Figure 3.8)
σ_{K_B}	0.6	0.7	1 standard deviation, measured
Nucletron Varian			
Total (2σ)	**2.4**	**2.5**	
Nucletron Varian			

In the uncertainty analysis of the RPC's original TLD mailed dosimeter program, Kirby *et al.*[64] established a ±5% acceptance criterion for institutional measurements based on an estimated uncertainty of 5% in TLD dose calculations at the 93% confidence level. With estimated standard deviations of 1.2% for both Nucletron and Varian measurements, a ±5% interval represents approximately 4 standard deviations in the dose measurements made in this work. Assuming that dose measurements from OSLDs are normally-distributed, greater than 99.99% of all measurements are expected to fall within 4 standard deviations of the mean. As a result, the accuracy of measurements made using the tool presented here exceeds that found by Kirby for the TLD program, so establishing a ±5% acceptance criterion for HDR measurements is appropriate.

4.5.1. Measured Uncertainty

In order to experimentally confirm the uncertainty analysis, the measured-to-expected dose ratios for 56 individual measurements were considered. This set included measurements made for various purposes during the course of this work, including data from trial remote audits.

For these data, the "expected" value is the expected dose as used in Equation 2.5 to determine dwell times, or, in the case of remote audits, the institutionally-reported dose from the treatment planning system. The "measured" dose is always the dose calculated using Equation 2.6 and OSLD readings. The breakdown of measurements between the two sources was 42 Nucletron, 14 Varian. The average measured-to-expected dose ratio for these 56 measurements was 1.001, the standard deviation was 0.009, and the standard error of the mean was 0.0013. The 2σ uncertainty of 1.9% is well within our predicted 2σ uncertainty of 2.5%. A histogram showing all 56 measurements is shown in Figure 4.3.

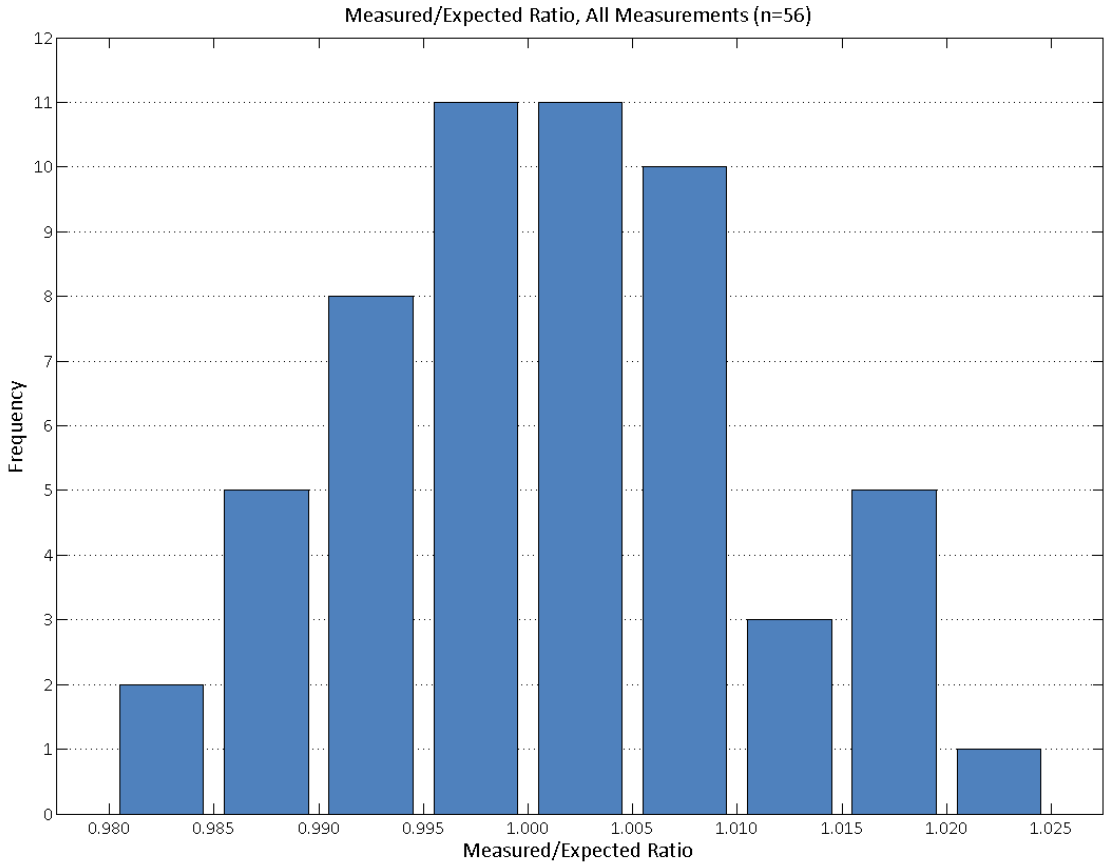

Figure 4.3: Histogram of measured-to-expected dose ratios for 56 individual measurements. The data fits a normal distribution with μ=1.001 and σ=0.009.

It is important to note that the data in Figure 4.3 include measurements used to calculate $K_B^{Nucletron}$ and K_B^{Varian}, and thus the histogram is biased in favor of values around unity. Excluding any data used to determine K_B leaves 26 measurements (22 Nucletron, 4 Varian). The average of the measured-to-expected ratios excluding K_B measurements was 1.002, the standard deviation

was 0.012, and the standard error of the mean was 0.002. Thus the 2σ uncertainty of the data excluding K_B measurements is 2.5%, which matches our predicted value.

As detailed previously, the average RPC-to-institution ratio for 193 RPC well chamber measurements was 1.009 with a standard deviation of 0.014. The values measured with the phantom described here compare favorably to those results.

4.5.2. Positional Uncertainty, Lateral Direction

The diameters of the Nucletron and Varian sources are 0.90 and 0.59 mm, respectively. While the inside diameter of 6 French catheters may vary by manufacturer and type, it is clear that there exists some latitude for movement of both the source inside the catheter and the catheter inside the phantom channel in the lateral direction (toward and away from the dosimeters).

By making some conservative assumptions about the physical dimensions of the phantom, we may estimate the maximum extent of lateral positioning deviation of the source. Let us assume that both the channel diameter and the OSLD slot width have an uncertainty of 5%, which indicates a maximum deviation of ±0.1 mm in the nominal 2.0 mm size of each. This assumed uncertainty is much higher than the quoted tolerance of the computer-controlled tools used to machine the phantom, which is ±0.001 inch, or approximately 0.025 mm. We also assume that the thickness of the catheter wall is negligible and that the source is essentially free to move laterally through the entire extent of the interior channel diameter. The assumptions are illustrated in Figure 4.4.

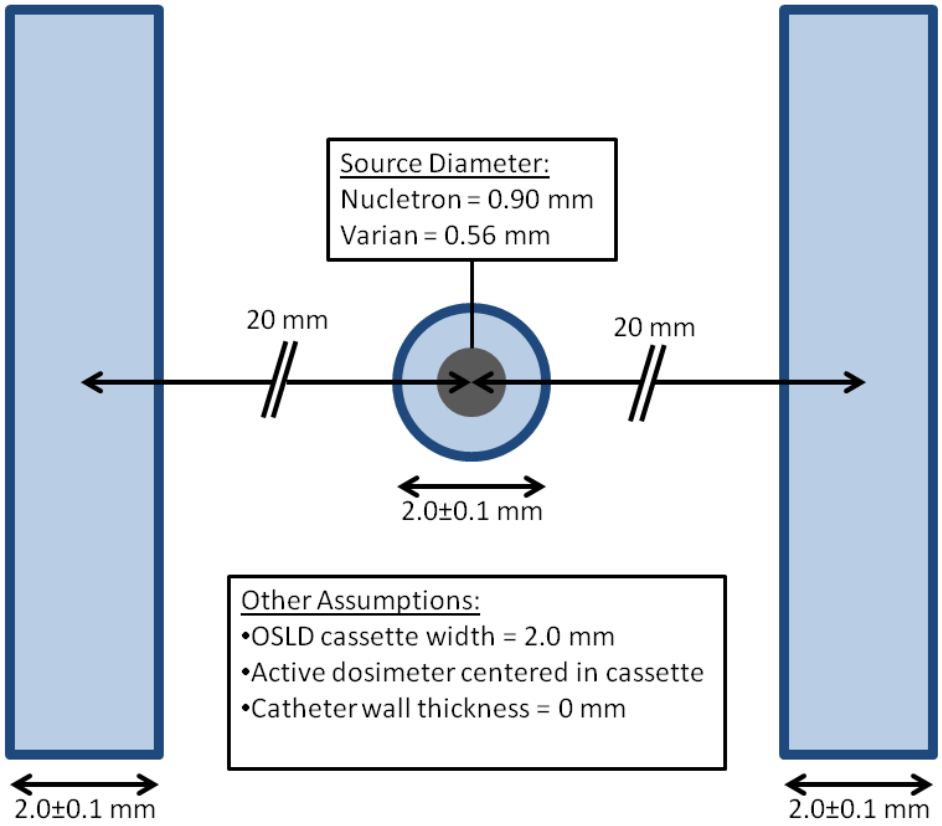

Figure 4.4: A cross-section of the interior of the phantom showing the assumptions made in order to calculate the maximum variance in lateral source positioning. The central channel and OSLD slots are shown in blue. The Ir-192 source is shown at center in gray. All sizes are to scale except for the channel-to-OSLD-slot distance (20 mm).

Because these first three assumptions are known to be extremely conservative, it was assumed that the distance from the center of the channel to the center of the OSLD slot is exactly 20 mm. Lastly, it was assumed that the nanoDot OSLD cassette was exactly 2 mm wide and that the active dosimeter is two-dimensional and centered along the cassette width. Combining all these assumptions, it is estimated that Nucletron and Varian sources may be 20±0.65 mm and 20±0.805 mm away from the active dosimeter, respectively.

Using TG-43 calculations, the effect of moving the sources laterally off a line which bisects the two OSLD slots was quantified. The results are shown in Figure 4.5. For a Nucletron source, moving the source 0.8 mm toward one dosimeter resulted in an increase of dose of more than 5% to that dosimeter. The other dosimeter, which the source was moved away from, saw a decrease in dose of approximately 5%. On their own, deviations in dose of this magnitude would be unacceptably high. However, it is here that the dual dosimeter design of the phantom offers an

advantage. Even with the source 0.8 mm off center, the *average* of the two dosimeter measurements is approximately 0.2% higher than the average with the source positioned perfectly between the dosimeters. The corresponding figure for a Varian source 0.8 mm off center was also approximately 0.2%. As the intended use of the tool always involves two dosimeters whose dose measurements are averaged together to obtain a final result, and the dosimeter slots cannot move in relation to each other or the channel, even extreme lateral variations in the source positioning are not expected to have a significant effect on dose measurements using the tool. This is an important consideration in the rationale to always consider the average of two dosimeters as a single measurement in this work.

Conversely, if one of the two dosimeters irradiated at the same time is unreadable or we are otherwise unable to average the two readings together, Figure 4.5 shows that the variation in dose received by the other (good) dosimeter may be as much as ±5%. In a scenario in which only one of the two dosimeters is readable, there is no method by which to reasonably estimate the actual dose received by the other dosimeter and the uncertainty introduced is too high to provide an accurate HDR audit. Thus any audit for which both dosimeters are not able to be read and averaged together must be considered unreliable and therefore discarded.

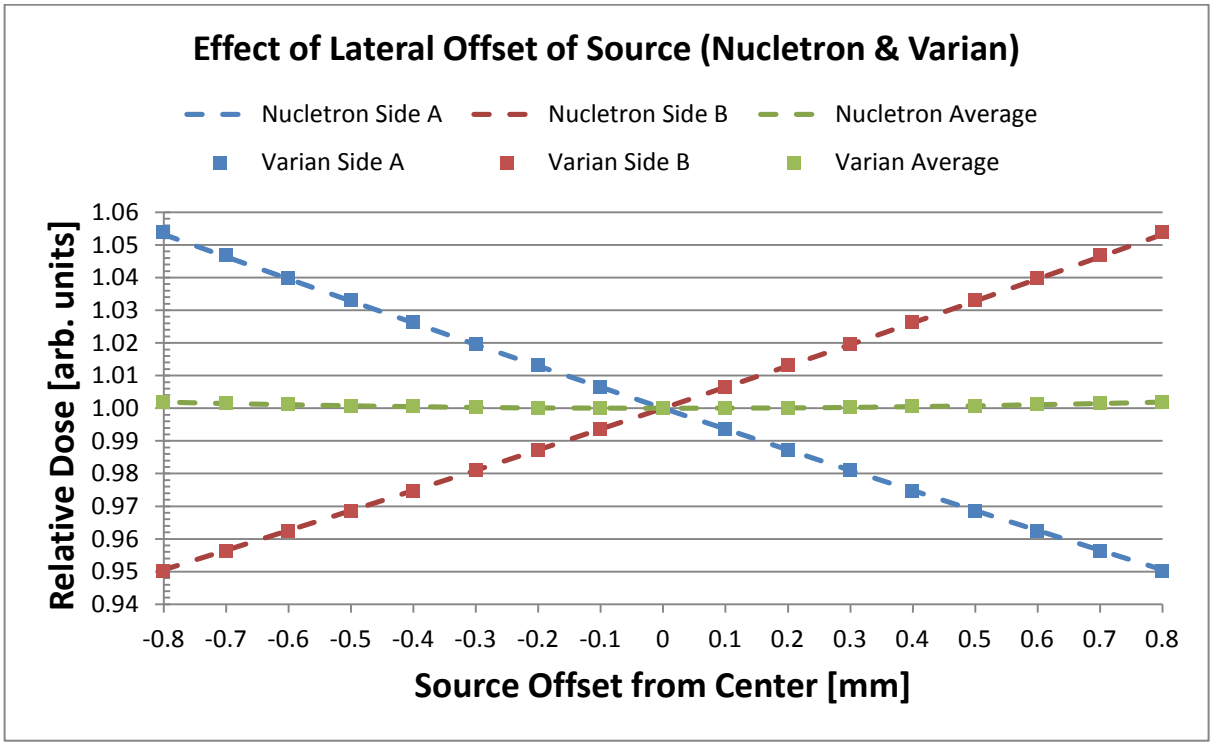

Figure 4.5: Effect on dose delivered to the OSLD points of measurement from moving the source laterally within the channel. Calculated using TG-43.

4.5.3. Timing Resolution Limitations

The Oncentra TCS software which controls the Nucletron afterloader allows a maximum resolution of 0.1 s in dwell times. Although the standard plan does not include any dwell times requiring greater resolution than this, in practice the plan is almost always scaled prior to irradiation using the current air-kerma strength of the source and Equation 2.5. This often necessitates dwell times which require greater resolution than 0.1 s in order to deliver the precise dose desired. However, the Oncentra software enforces the rounding all dwell times to the nearest tenth of a second.

In order to investigate the effect that such a limitation in timing resolution might have on dose measurement uncertainty, two worst-case scenarios were calculated using TG-43 and assuming a Nucletron source. First, the dose delivered to the point of measurement using a plan created by subtracting 0.05 s from each dwell time in the standard plan was calculated. In this case, the dose at the point of measurement was 99.40 cGy. Next, the dose delivered using a plan created by adding 0.05 s to each dwell time in the standard plan was calculated. This dose was 101.63 cGy.

The same TG-43 calculation using the standard plan with no modifications reports a dose at the point of measurement of 100.52 cGy. Thus, the subtraction and addition plans were -1.1% and +1.1% different from the expected dose using the unmodified plan, well within the estimated uncertainty of the system as a whole. As a rounding error of ±0.05 s in the same direction for each of the 10 dwell times represents a truly miraculous worst-case scenario, actual deviations in dose due to the software's timing resolution will likely be much smaller. Additionally, the calculations reported here assume a source strength of 40300 U, or approximately 10 Ci, which is approximately equal to the strength at which clinical ^{192}Ir sources are installed. As the majority of sources audited are likely to be weaker than this, the scaled dwell times used will necessarily be longer, and thus the loss of perhaps a few hundredths of a second due to rounding will have an even smaller effect than that reported here.

5. Conclusion

5.1. Hypothesis

The hypothesis of this work is as follows:

A mailable, OSLD-compatible ^{192}Ir HDR brachytherapy phantom suitable for RPC monitoring of clinical trial sites can be developed with the ability to measure HDR dose accurately to within ±5%.

We have shown that the proposed phantom design, when used with nanoDot OSL dosimeters, offers dose measurement accuracy of 2.4% and 2.5% for the Nucletron microSelectron-HDR v2 and Varian VS2000 ^{192}Ir sources, respectively, which are the two sources in current clinical use in the United States. This level of accuracy is superior to that of Kirby *et al.*[64] who established a ±5% acceptance criterion for the RPC's original mailed TLD external beam audit program. Therefore, the level of accuracy provided by the phantom described in this work is sufficient to establish that same criterion when comparing OSLD HDR dose measurements to institutionally-reported dose. Measurements made with this phantom tend to be on average closer to the expected (i.e., institutionally-reported) value and with a smaller standard deviation than well chamber measurements performed during RPC site visits.

Furthermore, the phantom and OSLD system has other properties which make it an acceptable tool for RPC mailed audits. It is manufactured from durable high-impact polystyrene and its size and weight allow it to be mailed to institutions for a cost of a few dollars. The OSL dosimeters used have been shown to have acceptably predictable time- and temperature-dependent fading properties through their current use in the RPC's external beam audit program.

Operationally, the phantom is designed to be simple and intuitive to use. The treatment plan requested of participating institutions is straightforward and the instructions are meant to be clear and concise. Physicists who have participated in trial audits without any guidance other than the included instructions have reported spending on the order of an hour in completion of the entire task of planning and irradiation.

5.2. Future Work

As the audit tool proposed here becomes a full RPC program used for monitoring of clinical trial sites, several future considerations will need to be made. First, the work here uses dosimeters from only a single batch of nanoDot dosimeters, known internally at the RPC as the "O4K09" batch. However, Al_2O_3:C dosimeters are known to have batch-specific properties, and the RPC currently uses unique linearity correction factors for each batch in use in its external beam audit programs. If the phantom produced by this work is to be used with other batches of nanoDot OSL dosimeters, a new linearity correction factor and block correction factor will need to be determined.

As mentioned previously, this work provides block correction factors for the two ^{192}Ir source models in current clinical use in the United States as of 2012. These correction factors differ by about 2.6%. If new source models are introduced to the market in the future, or the current models are revised substantially by their manufacturers, new block correction factors will need to be calculated to maintain the measurement accuracy of the system.

Interest in new brachytherapy dose calculation algorithms has increased in recent years as the current TG-43 paradigm has known limitations[65]. Specifically, research continues toward incorporating tissue heterogeneity corrections in to commercial HDR treatment planning systems. As such systems become prevalent in clinical use, the opportunity for a heterogeneous phantom which makes use of the advanced algorithms will arise. As the phantom proposed here is made of homogeneous material, it provides no opportunity for evaluating dose calculations incorporating heterogeneity corrections.

Finally, incorporating feedback gathered from the trial audits performed in this work, as well as feedback collected both formally and informally from participating institutions as the RPC initiates its HDR brachytherapy audit program, will allow the proposed phantom to continue to evolve into a more "user-friendly" tool. As improvements are made to both the phantom itself and the included instructions and forms, we may expect the accuracy and usefulness of the program to continue to increase as human mistakes and misunderstandings are minimized. The data and statistics collected from a full RPC program will offer further insight into the phantom's suitability as a tool which both the RPC and participating physicists can rely on for accurate HDR audits.

6. Appendix

6.1. Phantom Dimensions

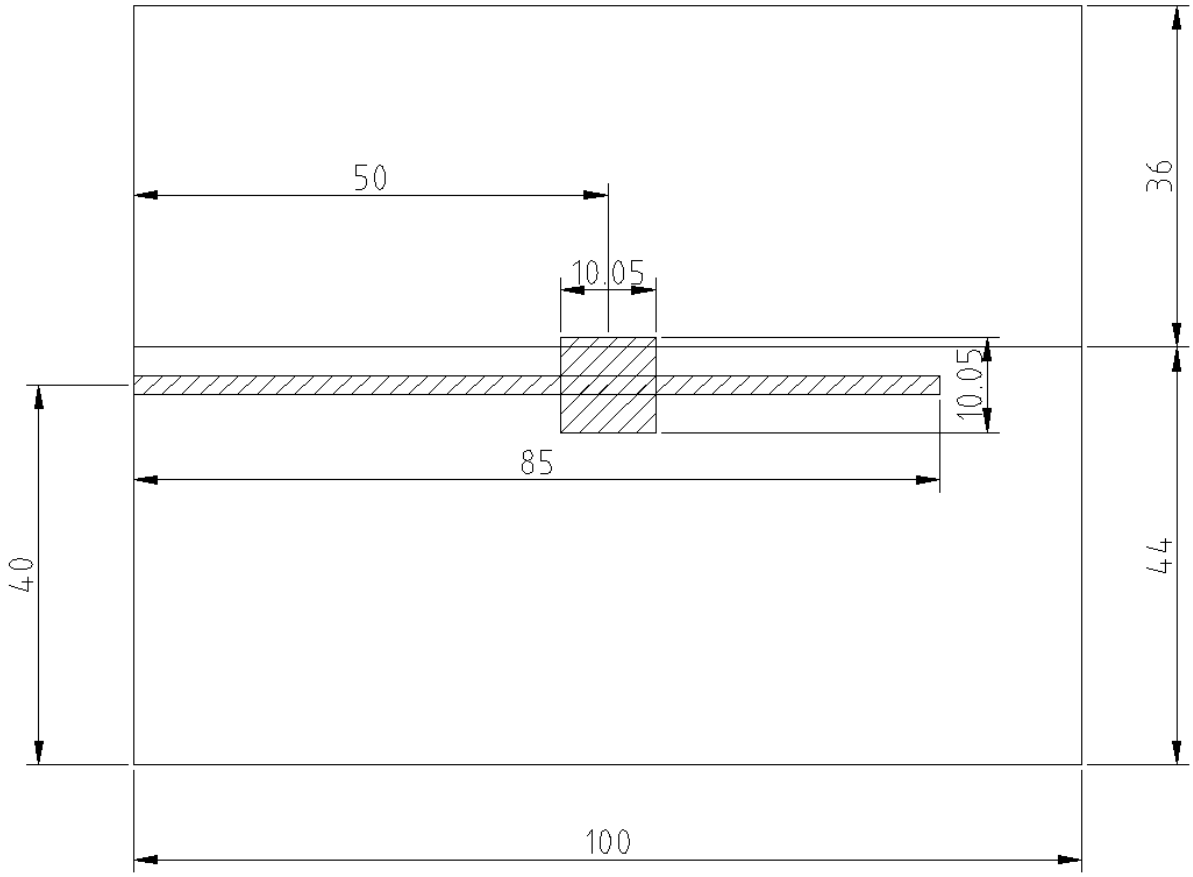

Figure 6.1: Cross-sectional view of phantom prototype, side view. Shaded areas represent voids forming the catheter channel and OSLD slot. All dimensions are in mm.

6.1. Phantom Dimensions (continued)

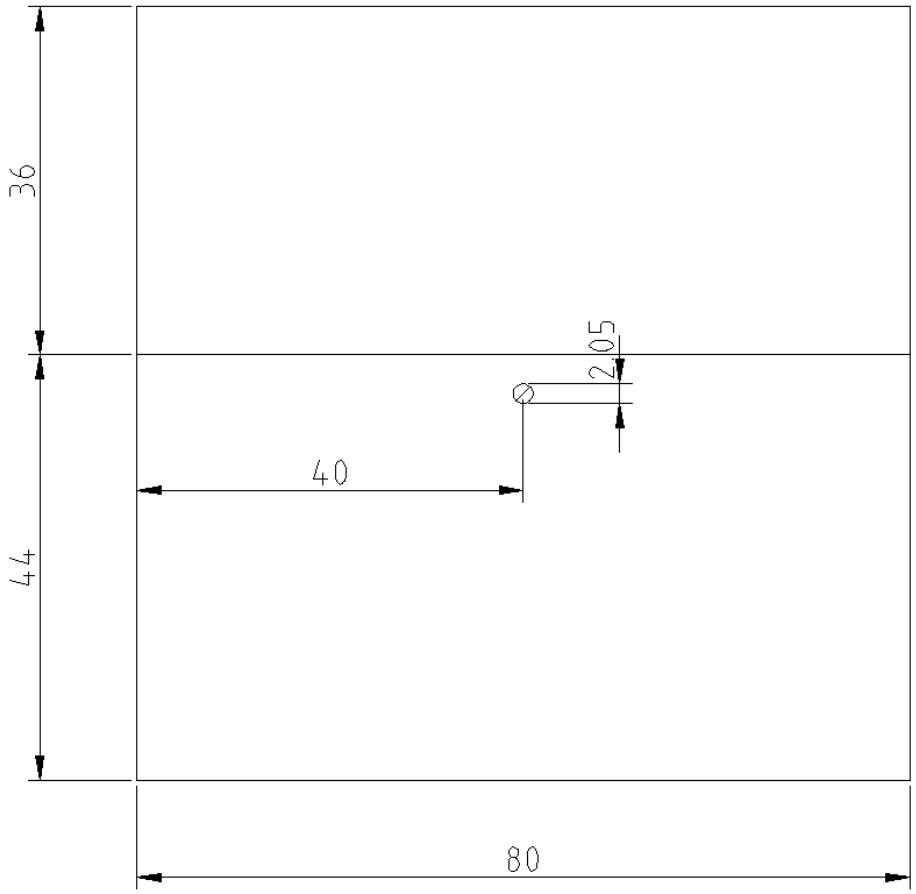

Figure 6.2: Phantom prototype front view. The shaded area at center is the opening of the catheter channel. All dimensions are in mm.

6.2. Calibration Reports

Using the formalism of DeWerd & Thomadsen, 1994 AAPM Summer School

Source Model	Nucletron microSelectron v2
Date	9/29/2011
Time	10:30 AM

Sk = I * Pelec * Ctp * Nrk * Aion * Pion

Sk	air-kerma strength	21549.186	U
I	measured current	55.377	rdg
Pelec	electrometer scale correction factor	1.000E-09	A/rdg
Ctp	temp & pressure correction factor	1.009	
Nrk	calibration factor for ion chamber (from ADCL)	3.859E+11	U/A
Aion	collection efficiency correction at calibration (from ADCL)	0.994	
Pion	collection efficiency correction at measurement	1.005	

Temperature	24	C
Pressure	758	mmHg
Ctp	1.009	

Distance [cm]	5.5	5	4.5	4	3.5	3	2.5
Position	23	21	19	17	15	13	11
Reading	53.34	54.70	55.26	55.36	55.07	54.33	53.13
	53.37	54.71	55.27	55.38	55.06	54.36	53.13
	53.37	54.69	55.28	55.39	55.08	54.37	53.11
Average	53.36	54.70	55.27	55.38	55.07	54.35	53.12
Std Dev	0.02	0.01	0.01	0.02	0.01	0.02	0.01
Max Reading							55.3767
Max Rdg Stdev							0.0153

6.2. Calibration Reports (continued)

Using the formalism of DeWerd & Thomadsen, 1994 AAPM Summer School

Source Model	Nucletron microSelectron v2
Date	1/9/2012
Time	5:08 PM

Sk = I * Pelec * Ctp * Nrk * Aion * Pion

Sk	air-kerma strength	21348.294	U
I	measured current	54.716	rdg
Pelec	electrometer scale correction factor	1.000E-09	A/rdg
Ctp	temp & pressure correction factor	1.012	
Nrk	calibration factor for ion chamber (from ADCL)	3.859E+11	U/A
Aion	collection efficiency correction at calibration (from ADCL)	0.994	
Pion	collection efficiency correction at measurement	1.005	

Temperature	24	C
Pressure	756	mmHg
Ctp	1.012	

Distance [cm]	5.5	5	4.5	4	3.5	3	2.5
Position	23	21	19	17	15	13	11
Reading	53.425	54.445	54.709	54.560	53.942	52.844	50.998
	53.533	54.472	54.719	54.540	53.884	52.688	50.953
	53.472	54.433	54.719	54.563	53.954	52.783	51.086
Average	53.477	54.450	54.716	54.554	53.927	52.772	51.012
Std Dev	0.05	0.02	0.01	0.01	0.04	0.08	0.07
Max Reading							54.7157
Max Rdg Stdev							0.0058

6.2. Calibration Reports (continued)

Using the formalism of DeWerd & Thomadsen, 1994 AAPM Summer School

Source Model	Nucletron microSelectron v2
Date	5/17/2012
Time	12:03 PM

Sk = I * Pelec * Ctp * Nrk * Aion * Pion

Sk	air-kerma strength	32726.678	U
I	measured current	84.460	rdg
Pelec	electrometer scale correction factor	1.000E-09	A/rdg
Ctp	temp & pressure correction factor	1.002	
Nrk	calibration factor for ion chamber (from ADCL)	3.859E+11	U/A
Aion	collection efficiency correction at calibration (from ADCL)	0.994	
Pion	collection efficiency correction at measurement	1.008	

Temperature	23.8	C
Pressure	763	mmHg
Ctp	1.002	

Distance [cm]	5.5	5	4.5	4	3.5	3	2.5
Position	23	21	19	17	15	13	11
Reading			84.437	84.248	83.430	81.903	79.212
	82.404	83.942	84.471	84.257	83.449	81.915	79.326
	82.442	83.969	84.472	84.264	83.418	81.855	79.216
Average	82.42	83.96	84.46	84.26	83.43	81.89	79.25
Std Dev	0.03	0.02	0.02	0.01	0.02	0.03	0.06
Max Reading							84.4600
Max Rdg Stdev							0.0080

6.2. Calibration Reports (continued)

Using the formalism of DeWerd & Thomadsen, 1994 AAPM Summer School

Source Model	Varian VS2000
Date	3/23/2012
Time	2:31 PM

Sk = I * Pelec * Ctp * Nrk * Aion * Pion

Sk	air-kerma strength	17960.939	U
I	measured current	47.172	rdg
Pelec	electrometer scale correction factor	1.000E-09	A/rdg
Ctp	temp & pressure correction factor	0.989	
Nrk	calibration factor for ion chamber (from ADCL)	3.859E+11	U/A
Aion	collection efficiency correction at calibration (from ADCL)	0.994	
Pion	collection efficiency correction at measurement	1.004	

Temperature	19	C
Pressure	760.9	mmHg
Ctp	0.989	

Distance [cm]	147	146.5	146	145.5	145	144.5	144
Reading	45.252	46.312	46.894	47.117	46.980	46.461	45.500
	45.416	46.400	46.977	47.187	47.023	46.486	45.523
	45.436	46.441	47.013	47.212	47.045	46.504	45.523
Average	45.37	46.38	46.96	47.17	47.02	46.48	45.52
Std Dev	0.10	0.07	0.06	0.05	0.03	0.02	0.01
Max Reading							47.1720
Max Rdg Stdev							0.0492

6.3. Remote Audit Forms

6.3.1. Instructions

Instructions for Irradiating OSL Dosimeters with HDR

Please find enclosed:

1.) One polystyrene miniphantom containing two OSL dosimeters. The phantom has a single channel with a plastic thumbscrew at its mouth as seen in Figure 1.
2.) An HDR OSLD Irradiation Form

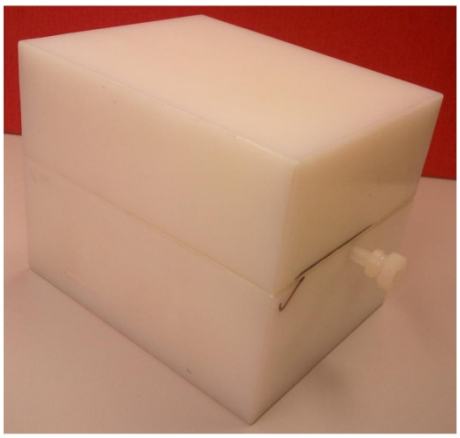

Figure 1: The HDR remote audit phantom.

General Audit Instructions:

1.) Set up, plan, and irradiate the OSLD as instructed below.
2.) The phantom contains sensitive dosimeters. Do not expose it to radiation until ready to deliver the plan described below.
3.) Fill out the enclosed Irradiation Form. Include a print-out of your treatment plan, showing the 100 cGy isodose line.
4.) Return the HDR remote audit phantom, Irradiation Form, and plan print-out to the RPC in a box. For your convenience, UPS shipping instructions and label are enclosed.
5.) Please try to irradiate and return the phantom within two weeks of its receipt.

Setup Instructions:

a) The two halves of the phantom should remain firmly pressed together at all times. Do not attempt to separate the phantom or remove the dosimeters.
b) Loosen but do not remove the thumbscrew.
c) Insert a single 2mm-diameter (6 French) catheter through the thumbscrew and into the channel. The distal end of the catheter should be positioned against the end of the channel. The other end of the catheter should be connected to your HDR unit.
d) Tighten the thumbscrew to secure the catheter in place. The thumbscrew should be snug enough to resist movement of the catheter, but not enough to inhibit the passage of the source. Make sure that the catheter does not get pulled out of the channel as the screw is tightened.

6.3.1. Instructions (continued)

e) During irradiation, the phantom may be placed in whatever orientation is convenient, as long as the two halves remain pressed together and the source can move freely within the catheter.

Planning and Irradiation Instructions:

a) Use 10 dwell positions, with 5 mm spacing.
b) Use only the most distal dwell positions available, skipping none.
c) Optimize dwell times individually for each dwell position in order to deliver **100 cGy** to a line located 2 cm away and parallel to the catheter channel. (see Figure 2)
d) Record the dose to a point 2 cm away from the center of the channel laterally and on a line bisecting the source train. ("Point A" in Figure 2)
e) Deliver the plan only once.
f) Record the dwell times and dose to "Point A" on the enclosed HDR OSLD Irradiation Form.
g) Print out a copy of your treatment plan showing the 100 cGy isodose line (additional isodose lines may be included if convenient) and include this print-out with the Irradiation Form.

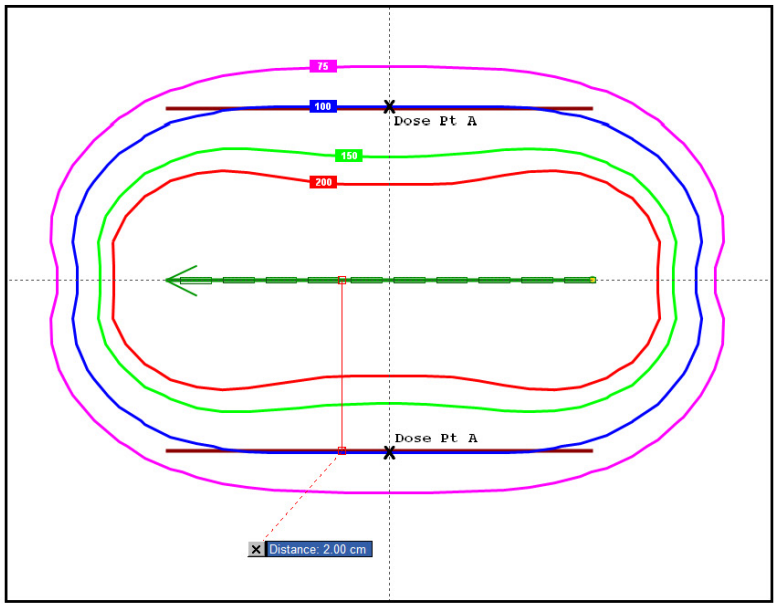

Figure 2: Example isodose lines for the HDR audit are shown above. Dwell times should be optimized to deliver 100 cGy along a line 2 cm away and parallel to the catheter channel. Additional non-100 cGy isodose lines are shown for illustrative purposes, and need not be matched by your plan exactly or included on the Irradiation Form. The dose Point A is located 2 cm away from the catheter channel laterally and along a line which bisects the source train. The dose at this point should be calculated during treatment planning and reported on the Irradiation Form.

6.3.2. Irradiation Form

RPC MD Anderson Radiological Physics Center

Radiological Physics Center
1515 Holcombe Blvd., Unit 607
Houston, TX 77030
Tel (713) 745-8989
Fax (713) 794-1364
Email: rpc@mdanderson.org
http://rpc.mdanderson.org

Ir-192 HDR OSLD Irradiation Form

	Correct?	
Institution Name: _____	☐ Yes	☐ No
Person to receive report: _____	☐ Yes	☐ No
Email Address of person to receive report: _____		
Person irradiating OSLD, if different from above: _____		
Phone Number: (____) _____ Email address: _____		
Person creating treatment plan, if different from above: _____		
Phone Number: (____) _____ Email address: _____		
For questions regarding OSLD irradiation, if different from above: _____		
Phone Number: (____) _____ Email address: _____		

Afterloader Manuf.: _____	Source Model: _____
In-House Designation: _____	Source Serial #: _____
Afterloader Model: _____	Date of Calibration: _____
Afterloader Serial #: _____	Activity at Calibration: _____ Ci
	Air Kerma Strength at Calib.: _____ μGy m^2 h^{-1}
Planning System: _____	Date of Irradiation: _____
Vendor: _____	Activity at Irradiation: _____ Ci
Version Number: _____	Air Kerma Strength at Irradiation: _____ μGy m^2 h^{-1}
Dose Calculation Algorithm: _____	

Enter plan dwell times (in seconds) in the spaces below:

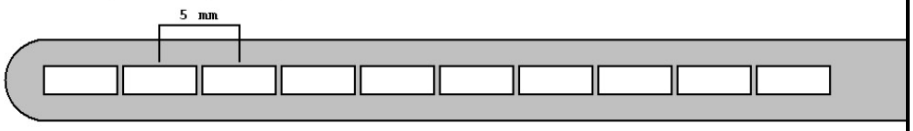

← Distal Proximal →

Using your Treatment Planning System, calculate the dose at a point 2.0 cm away from the center of the channel laterally and along a line bisecting the source train ("Point A"). Record the point dose below:

Point A Dose: _____ cGy

Include a print-out of your treatment plan showing the 100 cGy isodose line.

National Cancer Institute — *The RPC is an NCI-funded resource to cooperative group clinical trials.*

The University of Texas MD Anderson Cancer Center — Making Cancer History®

American Association of Physicists in Medicine — The AAPM provides scientific expertise and technical advice through the Therapy Physics Committee.

6.3.3. Questionnaire

HDR OSLD Audit Program Questionnaire

	Strongly Disagree	Somewhat Disagree	Neutral	Somewhat Agree	Strongly Agree
The instructions for setting up the phantom were clear and easy to understand.	1	2	3	4	5
The phantom itself was easy to use and intuitive in its operation and setup.	1	2	3	4	5
The instructions for treatment planning were clear and easy to understand.	1	2	3	4	5
The instructions for locating "Point A" and calculating the dose there were clear and easy to understand.	1	2	3	4	5
It was clear to me what information I needed to return to the RPC.	1	2	3	4	5
The Irradiation Form was easy to understand and complete.	1	2	3	4	5
The information requested on the irradiation form was relevant to the audit process.	1	2	3	4	5
The irradiation form included all of the items that I feel are necessary for the RPC to understand my system and procedure.	1	2	3	4	5
I understand the goals of this new RPC audit program.	1	2	3	4	5
I feel that the program offers an appropriate balance between ease-of-use and clinical relevancy.	1	2	3	4	5
My clinic would be interested in this tool as an independent audit program in the future.	1	2	3	4	5

Approximately how much time did you spend on planning, setup, and irradiation? _____

Please see back for additional comments.

6.3.3. Questionnaire (continued)

1.) Please include any additional comments or suggestions on **phantom setup and the setup instructions.**

2.) Please include any additional comments or suggestions on **treatment planning and the planning instructions.**

3.) Please include any additional comments or suggestions not covered above.

6.4. Remote Audit Questionnaire Results

Table 6.1: Respondents' scores for each of the statements on the trial audit questionnaire. 1 = "Strongly Disagree" and 5 = "Strongly Agree".

The instructions for setting up the phantom were clear and easy to understand.							
5	5	5	4	4	4	4	5
Average = 4.5			Median = 4.5			Standard Deviation = 0.5	
The phantom itself was easy to use and intuitive in its operation and setup.							
5	5	5	4	5	5	4	5
Average = 4.8			Median = 5			Standard Deviation = 0.5	
The instructions for treatment planning were clear and easy to understand.							
4	4	5	4	3	3	4	5
Average = 4.0			Median = 4			Standard Deviation = 0.8	
The instructions for locating "Point A" and calculating the dose there were clear and easy to understand.							
4	5	5	4		3	4	5
Average = 4.3			Median = 4			Standard Deviation = 0.8	
It was clear to me what information I needed to return to the RPC.							
5	5	5			3	4	5
Average = 4.5			Median = 5			Standard Deviation = 0.8	
The Irradiation Form was easy to understand and complete.							
5	5	5	4	5	3	4	5
Average = 4.5			Median = 5			Standard Deviation = 0.8	
The information requested on the Irradiation Form was relevant to the audit process.							
4	5	4	4	4	4	4	5
Average = 4.3			Median = 4			Standard Deviation = 0.5	
The Irradiation Form included all of the items that I feel are necessary for the RPC to understand my system and procedure.							
4	2	4	4	5	3	4	5
Average = 3.9			Median = 4			Standard Deviation = 1.0	
I understand the goals of this new RPC audit program.							
5	4	5	3	4	5	4	5
Average = 4.4			Median = 4.5			Standard Deviation = 0.7	
I feel that the program offers and appropriate balance between ease-of-use and clinical relevancy.							
4	2	5	4	5	5	4	5
Average = 4.3			Median = 4.5			Standard Deviation = 1.0	
My clinic would be interested in this tool as an independent audit program in the future.							
4	4	4	4	5	5	4	5
Average = 4.4			Median = 4			Standard Deviation = 0.5	

Table 6.2: Respondents' reported total time spent on planning, setup, and irradiation. All times in minutes.

Approximately how much time did you spend on planning, setup, and irradiation? (in minutes)							
30	60	60	60	90	120	15	120
Average = 69			Median = 60			Standard Deviation = 38	

6.4. Remote Audit Questionnaire Results (continued)

Table 6.3: Responses to the general comments/suggestions portion of the questionnaire.

Please include any additional comments or suggestions on phantom setup and the setup instructions.
The thumbscrew is difficult to tighten – never tightened enough to 'hold' catheter
Instructions were clear.
The thumbscrew did not hold my catheter in place so I had to fix it with tape. It would be helpful to know the distance from the tip of the thumbscrew to the end point in the phantom so I could verify that the catheter was inserted all the way.
The catheter was a little difficult to push all the way in.
It would help if the RPC provided a standard catheter without the connector. We did not have the 6 French but had one close to it. The clamp does not really work for sizes other than 6 French.
I didn't realize that we would be inserting the catheter and it was sort of lucky that we had the proper size on hand.
Please include any additional comments or suggestions on treatment planning and the planning instructions.
Used planning optimization method typically used in our clinic – opt. to dose points. Reading instructions again – did not optimize each dwell position individually.
Item b): Most distal dwell positions available is a bit vague. What do you mean by "available"? is the part that's not very clear. Depending on the RAL & the transfer tubes used, this can impact 1st dwell (most distal according to your diagram) location that is "available" – perhaps this doesn't have much bearing on what you're doing. Why don't you ask for the setback of 1st dwell location on irradiation form. You get this w/ the plan printout, so perhaps not necessary. c): You can define 10 dwells, but depending on how one optimizes one may actually have less than 10 "active" dwells – since you don't say that there must be 10 "active", then one can interpret as less than 10 "active" being okay. Is this what you want?
Some people may not know how to achieve the dose distribution asked for. In our clinic we only use IPSA optimization for planning clinically (inverse planning). Had I not attended the Nucletron training, I would not have known how to plan this. Also, as far as I know, there is several ways to achieve it, not sure if it matters how we go about planning though. The directions seemed more written for BrachyVision.
It would help if the RPC provided dwell times instead of letting the "planner" come up with a plan that mimics as close as possible the desired dose distribution. Dwell times can easily be scaled using ratios of activity to get the desired dose. This way you eliminate any planning ambiguities.

6.4. Remote Audit Questionnaire Results (continued)

Table 6.3: Responses to the general comments/suggestions portion of the questionnaire (continued).

Please include any additional comments or suggestions not covered above.
What are you hoping to achieve – a purpose statement would be good. What are the goals? As we move towards heterogeneity corrections being included it would be cool to have a phantom that has this being evaluated as well. I'm sure this is already being considered, etc.
Overall, I thought this was a relatively easy test to plan and perform and that the instructions were well thought out.
Some users may have Acuros/Monte Carlo based systems to correct for heterogeneities. Perhaps you could consider such users in the design/instructions/planning notes in the future. All in all, the device/jig is pretty easy to use and small enough to mail/handle. A cylindrical design could be better when considering gyn applicators/balloons/tandems, … etc to mimic the applicators being used in the clinic.

References

1. G. S. Ibbott, W. F. Hanson, E. O'Meara, R. R. Kuske, D. Arthur, R. Rabinovitch, J. White, R. M. Wilenzick, I. Harris and R. C. Tailor, "Dose specification and quality assurance of radiation therapy oncology group protocol 95-17; a cooperative group study of iridium-192 breast implants as sole therapy," Int J Radiat Oncol Biol Phys **69**, 1572-1578 (2007).
2. W. Small, Jr., K. Winter, C. Levenback, R. Iyer, D. Gaffney, S. Asbell, B. Erickson, A. Jhingran and K. Greven, "Extended-field irradiation and intracavitary brachytherapy combined with cisplatin chemotherapy for cervical cancer with positive para-aortic or high common iliac lymph nodes: results of ARM 1 of RTOG 0116," Int J Radiat Oncol Biol Phys **68**, 1081-1087 (2007).
3. I. C. Hsu, K. Bae, K. Shinohara, J. Pouliot, J. Purdy, G. Ibbott, J. Speight, E. Vigneault, R. Ivker and H. Sandler, "Phase II trial of combined high-dose-rate brachytherapy and external beam radiotherapy for adenocarcinoma of the prostate: preliminary results of RTOG 0321," Int J Radiat Oncol Biol Phys **78**, 751-758 (2010).
4. J. Aguirre, P. Alvarez, D. Followill, G. Ibbott, C. Amador and A. Tailor, "SU-FF-T-306: Optically Stimulated Light Dosimetry: Commissioning of An Optically Stimulated Luminescence (OSL) System for Remote Dosimetry Audits, the Radiological Physics Center Experience," Med Phys **36**, 2591 (2009).
5. J. Homnick, G. Ibbott, A. Springer and J. Aguirre, "TH-D-352-05: Optically Stimulated Luminescence (OSL) Dosimeters Can Be Used for Remote Dosimetry Services," Med Phys **35**, 2994 (2008).
6. J. Aguirre, P. Alvarez, C. Amador, A. Tailor, D. Followill and G. Ibbott, "WE-D-BRB-08: Validation of the Commissioning of an Optically Stimulated Luminescence (OSL) System for Remote Dosimetry Audits " Med Phys **37**, 3428 (2010).
7. J. Aguirre, P. Alvarez, G. Ibbott and D. Followill, "SU-E-T-126: Analysis of Uncertainties for the RPC Remote Dosimetry Using Optically Stimulated Light Dosimetry (OSLD)," Med Phys **38**, 3515 (2011).
8. P. Alvarez, J. Aguirre and D. Followill, "SU-E-T-86: Evaluation of the OSLD System for Remote Dosimetry Audits Implemented by the RPC," Med Phys **38**, 3505 (2011).

9. C. E. Andersen, S. K. Nielsen, S. Greilich, J. Helt-Hansen, J. C. Lindegaard and K. Tanderup, "Characterization of a fiber-coupled Al2O3:C luminescence dosimetry system for online in vivo dose verification during 192Ir brachytherapy," Med Phys **36**, 708-718 (2009).
10. P. A. Jursinic, "Characterization of optically stimulated luminescent dosimeters, OSLDs, for clinical dosimetric measurements," Med Phys **34**, 4594-4604 (2007).
11. P. A. Jursinic, "Changes in optically stimulated luminescent dosimeter (OSLD) dosimetric characteristics with accumulated dose," Med Phys **37**, 132-140 (2010).
12. R. Ochoa, F. Gomez, I. H. Ferreira, F. Gutt and C. E. de Almeida, "Design of a phantom for the quality control of high dose rate 192Ir source used in brachytherapy," Radiother Oncol **82**, 222-228 (2007).
13. A. Roue, J. L. Venselaar, I. H. Ferreira, A. Bridier and J. Van Dam, "Development of a TLD mailed system for remote dosimetry audit for (192)Ir HDR and PDR sources," Radiother Oncol **83**, 86-93 (2007).
14. P. J. Muench, A. S. Meigooni, R. Nath and W. L. McLaughlin, "Photon energy dependence of the sensitivity of radiochromic film and comparison with silver halide film and LiF TLDs used for brachytherapy dosimetry," Med Phys **18**, 769-775 (1991).
15. B. S. Hilaris, D. A. Mastoras, L. L. Shih and W. R. Bodner, "History of Brachytherapy: The Years After the Discovery of Radium and Radioactivity," in *Principles and Practice of Brachytherapy,* edited by S. Nag (Futura, Armonk, 1997), pp. 13-26.
16. J. F. Williamson, "Brachytherapy technology and physics practice since 1950: a half-century of progress," Phys Med Biol **51**, R303-325 (2006).
17. International Commission on Radiological Units and Measurements., *Dose and volume specification for reporting intracavitary therapy in gynecology*. (ICRU, Bethesda, Md., U.S.A., 1985).
18. R. B. Firestone and L. P. Ekstrom, "WWW Table of Radioactive Isotopes," *Vol. 2011,* (2004).
19. R. Nath, L. L. Anderson, G. Luxton, K. A. Weaver, J. F. Williamson and A. S. Meigooni, "Dosimetry of interstitial brachytherapy sources: recommendations of the AAPM Radiation Therapy Committee Task Group No. 43. American Association of Physicists in Medicine," Med Phys **22**, 209-234 (1995).
20. S. Nag, *High dose rate brachytherapy : a textbook*. (Futura, New York, 1994).
21. F. M. Khan, *The physics of radiation therapy*, 4th ed. (Lippincott Williams & Wilkins, Philadelphia, 2010).

22. B. Erickson, P. Eifel, J. Moughan, J. Rownd, T. Iarocci and J. Owen, "Patterns of brachytherapy practice for patients with carcinoma of the cervix (1996-1999): a patterns of care study," Int J Radiat Oncol Biol Phys **63**, 1083-1092 (2005).

23. A. N. Viswanathan, C. L. Creutzberg, P. Craighead, M. McCormack, T. Toita, K. Narayan, N. Reed, H. Long, H. J. Kim, C. Marth, J. C. Lindegaard, A. Cerrotta, W. Small, Jr. and E. Trimble, "International brachytherapy practice patterns: a survey of the Gynecologic Cancer Intergroup (GCIG)," Int J Radiat Oncol Biol Phys **82**, 250-255 (2012).

24. Z. A. Husain, U. Mahmood, A. Hanlon, G. Neuner, R. Buras, K. Tkaczuk and S. J. Feigenberg, "Accelerated partial breast irradiation via brachytherapy: a patterns-of-care analysis with ASTRO consensus statement groupings," Brachytherapy **10**, 479-485 (2011).

25. S. Nag, J. B. Owen, N. Farnan, T. F. Pajak, A. Martinez, A. Porter, J. Blasko and L. B. Harrison, "Survey of brachytherapy practice in the United States: a report of the Clinical Research Committee of the American Endocurietherapy Society," Int J Radiat Oncol Biol Phys **31**, 103-107 (1995).

26. V. Gondi, J. R. Bernard, Jr., S. Jabbari, J. Keam, K. L. de Amorim Bernstein, L. K. Dad, L. Li, M. M. Poppe, J. B. Strauss and C. T. Chollet, "Results of the 2005-2008 Association of Residents in Radiation Oncology survey of chief residents in the United States: clinical training and resident working conditions," Int J Radiat Oncol Biol Phys **81**, 1120-1127 (2011).

27. G. S. Ibbott, "QA in Radiation Therapy: The RPC Perspective," Journal of Physics: Conference Series **250** (2010).

28. T. H. Kirby, W. F. Hanson, R. J. Gastorf, C. H. Chu and R. J. Shalek, "Mailable TLD system for photon and electron therapy beams," International journal of radiation oncology, biology, physics **12**, 261-265 (1986).

29. G. S. Ibbott, "MO-A-BRA-01: Credentialing for Clinical Trials," Med Phys **37**, 3334 (2010).

30. D. Followill, J. R. Lowenstein, L. Palmer and G. Ibbott, "SU-FF-T-320: The Radiological Physics Center's Annual TLD Machine Calibration Audit and Its Impact on Clinical Trials," Med Phys **36**, 2595 (2009).

31. G. S. Ibbott, D. S. Followill, H. A. Molineu, J. R. Lowenstein, P. E. Alvarez and J. E. Roll, "Challenges in credentialing institutions and participants in advanced technology multi-institutional clinical trials," Int J Radiat Oncol Biol Phys **71**, S71-75 (2008).

32. V. V. Antonov-Romanovskii, I. B. Keirum-Marcus, M. S. Poroshina and Z. A. Trapeznikova, presented at the Conference of the Academy of Sciences of the USSR on the Peaceful Uses of Atomic Energy, Moscow, 1955 (unpublished).
33. M. S. Akselrod, "Fundamentals of Materials, Techniques, and Instrumentation for OSL and FNTD Dosimetry," Aip Conf Proc **1345**, 274-302 (2011).
34. M. S. Akselrod, V. S. Kortov, D. J. Kravetsky and V. I. Gotlib, "Highly Sensitive Thermoluminescent Anion-Defective Alpha-Al2o3-C Single-Crystal Detectors," Radiat Prot Dosim **32**, 15-20 (1990).
35. J. K. Rieke and F. Daniels, "Thermoluminescence studies of aluminum oxide," Journal of Physical Chemistry **61**, 629-633 (1957).
36. G. F. Knoll, *Radiation detection and measurement*, 3rd ed. (Wiley, New York, 2000).
37. R. H. Bube, *Photoconductivity of solids*. (Wiley, New York,, 1960).
38. E. G. Yukihara and S. W. McKeever, "Optically stimulated luminescence (OSL) dosimetry in medicine," Phys Med Biol **53**, R351-379 (2008).
39. C. E. Andersen, M. C. Aznar, L. Bøtter-Jensen, S. Å. J. Bäck, S. Mattsson and J. Medin, presented at the Int. Symp. on Standards and Codes of Practice in Medical Radiation Dosimetry, Vienna, 2003 (unpublished).
40. M. C. Aznar, C. E. Andersen, L. Botter-Jensen, S. A. Back, S. Mattsson, F. Kjaer-Kristoffersen and J. Medin, "Real-time optical-fibre luminescence dosimetry for radiotherapy: physical characteristics and applications in photon beams," Phys Med Biol **49**, 1655-1669 (2004).
41. J. C. Polf, E. G. Yukihara, M. S. Akselrod and S. W. S. McKeever, "Real-time luminescence from Al2O3 fiber dosimeters," Radiat Meas **38**, 227-240 (2004).
42. K. H. Lee and J. H. Crawford, "Luminescence of the F-Center in Sapphire," Phys Rev B **19**, 3217-3221 (1979).
43. E. G. Yukihara and S. W. S. McKeever, "Spectroscopy and optically stimulated luminescence of Al2O3 : C using time-resolved measurements," J Appl Phys **100** (2006).
44. A. J. J. Bos, "High sensitivity thermoluminescence dosimetry," Nucl Instrum Meth B **184**, 3-28 (2001).
45. J. Perez-Calatayud, D. Granero and F. Ballester, "Phantom size in brachytherapy source dosimetric studies," Med Phys **31**, 2075-2081 (2004).
46. A. C. Tedgren and G. A. Carlsson, "Influence of phantom material and dimensions on experimental (192)Ir dosimetry," Med Phys **36**, 2228-2235 (2009).

47. G. M. Daskalov, E. Loffler and J. F. Williamson, "Monte Carlo-aided dosimetry of a new high dose-rate brachytherapy source," Med Phys **25**, 2200-2208 (1998).

48. L. A. DeWerd and B. R. Thomadsen, "Source Strength Standards and Calibration of HDR/PDR Sources," in *Brachytherapy Physics: 1994 AAPM Summer School,* edited by J. F. Williamson, B. R. Thomadsen and R. Nath (Medical Physics Publishing Corp., Madison, WI, 1995), pp. 541-555.

49. A. Angelopoulos, P. Baras, L. Sakelliou, P. Karaiskos and P. Sandilos, "Monte Carlo dosimetry of a new 192Ir high dose rate brachytherapy source," Med Phys **27**, 2521-2527 (2000).

50. R. E. P. Taylor and D. W. O. Rogers, "An EGSnrc Monte Carlo-calculated database of TG-43 parameters," Med Phys **35**, 4228-4241 (2008).

51. S. W. S. McKeever, M. S. Akselrod and B. G. Markey, "Pulsed optically stimulated luminescence dosimetry using alpha-Al2O3:C," Radiat Prot Dosim **65**, 267-272 (1996).

52. R. Hill, Z. Kuncic and C. Baldock, "The water equivalence of solid phantoms for low energy photon beams," Med Phys **37**, 4355-4363 (2010).

53. J. A. Meli, A. S. Meigooni and R. Nath, "On the choice of phantom material for the dosimetry of 192Ir sources," International journal of radiation oncology, biology, physics **14**, 587-594 (1988).

54. J. R. Kerns, S. F. Kry, N. Sahoo, D. S. Followill and G. S. Ibbott, "Angular dependence of the nanoDot OSL dosimeter," Med Phys **38**, 3955-3962 (2011).

55. D. S. Followill, D. R. Evans, C. Cherry, A. Molineu, G. Fisher, W. F. Hanson and G. S. Lbbott, "Design, development, and implementation of the Radiological Physics Center's pelvis and thorax anthropomorphic quality assurance phantoms," Med Phys **34**, 2070-2076 (2007).

56. D. Caruthers, G. Ibbott, A. Shiu, E. Chang, R. White and D. Followill, "SU-GG-T-552: Commissioning an Anthropomorphic Spine and Lung Phantom for Remote Quality Assurance of Spinal Radiosurgery," Med Phys **37**, 3314 (2010).

57. International Commission on Radiation Units and Measurements., *Tissue substitutes in radiation dosimetry and measurement*. (International Commission on Radiation Units and Measurements, Bethesda, Md., U.S.A., 1989).

58. M. Tod and W. J. Meredith, "Treatment of cancer of the cervix uteri, a revised Manchester method," Br J Radiol **26**, 252-257 (1953).

59. J. Cho, P. Alvarez, D. Followill, M. Gillin and G. Ibbott, "SU-E-T-153: Proton Linearity and Energy Dependence Studies of Optically Stimulated Luminescent Detectors for Remote

Audits of Proton Beam Calibrations by the Radiological Physics Center," Med Phys **38**, 3521 (2011).

60. M. J. Rivard, D. Granero, J. Perez-Calatayud and F. Ballester, "Influence of photon energy spectra from brachytherapy sources on Monte Carlo simulations of kerma and dose rates in water and air," Med Phys **37**, 869-876 (2010).
61. B. E. Rasmussen, S. D. Davis, C. R. Schmidt, J. A. Micka and L. A. Dewerd, "Comparison of air-kerma strength determinations for HDR (192)Ir sources," Med Phys **38**, 6721-6729 (2011).
62. E. G. Yukihara, G. Mardirossian, M. Mirzasadeghi, S. Guduru and S. Ahmad, "Evaluation of Al2O3 : C optically stimulated luminescence (OSL) dosimeters for passive dosimetry of high-energy photon and electron beams in radiotherapy," Med Phys **35**, 260-269 (2008).
63. L. Karsch, E. Beyreuther, T. Burris-Mog, S. Kraft, C. Richter, K. Zeil and J. Pawelke, "Dose rate dependence for different dosimeters and detectors: TLD, OSL, EBT films, and diamond detectors," Med Phys **39**, 2447-2455 (2012).
64. T. H. Kirby, W. F. Hanson and D. A. Johnston, "Uncertainty analysis of absorbed dose calculations from thermoluminescence dosimeters," Med Phys **19**, 1427-1433 (1992).
65. M. J. Rivard, J. L. M. Venselaar and L. Beaulieu, "The evolution of brachytherapy treatment planning," Med Phys **36**, 2136-2153 (2009).

Vita

Kevin Casey was born on March 20, 1984 in Arlington, Texas to Terry and Patti Casey. He graduated from the University of Texas at Austin in 2007 with a Bachelor of Science degree in Physics. He earned a Bachelor of Arts degree in Liberal Arts from the same university in 2009. In August 2010 he entered the Specialized Master of Science in Medical Physics program at the University of Texas Health Science Center at Houston Graduate School of Biomedical Sciences in conjunction with the University of Texas M.D. Anderson Cancer Center. He is married to Sara Casey and enjoys backpacking, following college football, and listening to jazz music in his free time.